Characterizing unforced multi-decadal variability of ENSO:

A case study with the GFDL CM2.1 coupled GCM

A. R. Atwood[1]*, D. S. Battisti[2], A. T. Wittenberg[3], W. H. G. Roberts[4], D. J. Vimont[5]

[1]*UC Berkeley, Geography Dept., Berkeley, CA 94709, USA*

[2] *University of Washington, Dept. of Atmospheric Sciences, Seattle, WA 98195, USA*

[3] *NOAA Geophysical Fluid Dynamics Laboratory, Princeton, NJ*

[4] *School of Geographical Sciences, University of Bristol, Bristol, BS8 1SS, UK*

[5]*University of Wisconsin-Madison, Atmospheric and Oceanic Sciences Dept., Madison, WI 53705, USA*

* Corresponding author. Tel: +1 206-694-3143; fax: +1 206-6853351

E-mail address: aatwood@berkeley.edu (Alyssa Atwood).

Acknowledgements

This material is based upon work supported by the National Science Foundation Graduate Research Fellowship Program, the Department of Energy Global Change Education Program and the National Oceanic and Atmospheric Administration Climate and Global Change Postdoctoral Program under fellowships to A. Atwood. Support was provided to D. S. Battisti by the Tamaki Foundation. We thank C. Thompson and J. Leloup for their LOAM code and T. Russon for useful discussions that improved this manuscript.

ABSTRACT

Large multi-decadal fluctuations of El Nino-Southern Oscillation (ENSO) variability simulated in a 4,000-year pre-industrial control run of GFDL CM2.1 have received considerable attention due to implications for constraining the causes of past and future changes in ENSO. We evaluated the mechanisms of this low-frequency ENSO modulation through analysis of the extreme epochs of CM2.1 as well as through the use of a linearized intermediate-complexity model of the tropical Pacific, which produces reasonable emulations of observed ENSO variability. We demonstrate that the low-frequency ENSO modulation can be represented by the simplest model of a linear, stationary process, even in the highly nonlinear CM2.1. These results indicate that CM2.1's ENSO modulation is driven by transient processes that operate at time scales that are interannual or shorter. Nonlinearities and/or multiplicative noise in CM2.1 likely exaggerate the ENSO modulation by contributing to the overly active ENSO variability. In contrast, simulations with the linear model demonstrate that intrinsically-generated tropical Pacific decadal mean state changes do not contribute to the extreme-ENSO epochs in CM2.1. Rather, these decadal mean state changes actually serve to *damp* the intrinsically-generated ENSO modulation, primarily by stabilizing the ENSO mode during strong-ENSO epochs. Like most coupled General Circulation Models, CM2.1 suffers from large biases in its ENSO simulation, including ENSO variance that is nearly twice that seen in the last 50 years of observations. We find that CM2.1's overly strong ENSO variance directly contributes to its strong multi-decadal modulation through broadening the distribution of epochal variance, which increases like the square of the long-term variance. These results suggest that the true spectrum of unforced ENSO modulation is likely substantially narrower than that in CM2.1. However, *relative* changes in ENSO modulation are similar between CM2.1, the linear model tuned to CM2.1, and the linear model tuned to observations, underscoring previous findings that *relative* changes in ENSO variance can robustly be compared across models and observations.

Keywords: ENSO; multi-decadal variability; GFDL CM2.1; linearized model; nonlinear feedbacks

1. Introduction

The decadal- and longer-scale modulation of ENSO is a critical element of past and future climate variations, yet it is poorly constrained by the short observational record (Capotondi et al., 2015; Wittenberg, 2015). ENSO variability is thought to have exhibited large changes over the Holocene (Cobb et al., 2013; Koutavas et al., 2006; McGregor et al., 2013; Tudhope et al., 2001), however it is not yet known to what extent these variations are forced, versus inherent to a noisy coupled ocean-atmosphere system. This uncertainty arises in part from poor observational constraints on the unforced intrinsic component of ENSO modulation on multi-decadal and longer timescales.

Given the short observational record of tropical Pacific climate variability, long unforced simulations of the climate system with fully coupled General Circulation Models (GCMs) are helpful for investigating ENSO variability on decadal and longer timescales (Russon et al., 2014; Wittenberg, 2009). A 4,000 year-long pre-industrial control run of GFDL CM2.1 (Delworth et al., 2006; Wittenberg et al., 2006) has been shown to exhibit strong, unforced, largely unpredictable, multi-decadal changes in ENSO variability (Karamperidou et al., 2014; Kug et al., 2010; Wittenberg, 2009; Wittenberg et al., 2014), which also influence the background climatological state of the tropical Pacific (Ogata et al., 2013). These large low-frequency ENSO modulations suggest that in order to detect a forced change in ENSO variability (e.g. from paleoclimate proxies or observations), long records are needed.

However, large ENSO biases prevalent in GCMs obscure the real-world relevance of the tropical climate variability obtained from GCM simulations (Guilyardi, in press). GCMs used in the Fourth and Fifth Assessment Reports of the Intergovernmental Panel on Climate Change exhibit a wide range of biases in their representation of ENSO variability, including biases in the amplitude of variance, spatial pattern of SST variability, distribution of ENSO SST anomalies, and seasonal synchronization of ENSO (An and Wang, 2000; Bellenger et al., 2014; Capotondi et al., 2015; Graham et al., 2016; Guilyardi et al., 2012a; Guilyardi et al., 2012b; Guilyardi et al., 2009), which has resulted in little agreement on how ENSO is likely to change in the future (Cai et al., 2014; Chen et al., 2016; Collins et al., 2010; DiNezio et al., 2012; Taschetto et al., 2014; Watanabe et al., 2012). The sources of these ENSO biases are largely unknown, but likely result partly from mean state biases in the models. In this study, we investigate the sources of the

low-frequency ENSO modulation by performing further analyses of ENSO in the CM2.1 control run, observations, and that simulated by a linearized intermediate model of the tropical Pacific. Through this process, we evaluate the influence of the overly active interannual variability in CM2.1 on the interdecadal modulation of ENSO in an effort to improve constraints on the true spectral characteristics of ENSO in nature.

Because the CM2.1 control simulation is unforced, there are essentially four, non mutually exclusive, mechanisms that could cause the large multi-decadal ENSO variability: (1) low frequency changes in the tropical Pacific mean state, which alter the stability of the ENSO system; (2) low frequency changes in stochastic (weather) processes that influence ENSO; (3) random sampling from a stationary, linear process; and (4) nonlinear dynamics, including multiplicative noise, in the ENSO system that spreads variance over a range of time scales. Using the linear model, we show that linear dynamics acting in response to low frequency changes in the tropical Pacific mean state are not the source of low-frequency ENSO modulation in CM2.1. While the influence of low frequency changes in stochastic noise is difficult to address using the suite of tools employed in this analysis, we demonstrate using the linear model runs, CM2.1, and observations that random variations associated with a stationary, linear process are important. Our analyses lead us to conclude that the nonlinearities are also inextricably linked to the multi-decadal ENSO modulation in CM2.1, and while they do not dramatically broaden the distribution of variance as compared to a linear system with equal (i.e. overly active) ENSO variability, they likely shape the distribution of absolute ENSO modulation by contributing to the overly active ENSO variability.

2. Description of the linearized model

The Linearized Ocean Atmosphere Model (LOAM; Thompson and Battisti, 2000) is a linearized variant of the (Zebiak and Cane, 1987) intermediate complexity model of the tropical Pacific, updated to include observationally constrained parameter values and observed climatological mean state fields, including ocean currents and vertical thermal structure (Thompson, 1998; Roberts, 2007). LOAM is constructed as an anomaly model, such that it calculates the anomalies of its state variables about a set of prescribed mean states. These mean state variables determine the details of the behavior of ENSO in the

111 model. Because the mean states are explicitly prescribed in the model, it is an ideal tool to investigate how
112 changes in these mean states can alter the behavior of ENSO. Indeed it has been shown (Roberts and
113 Battisti, 2011; Roberts et al., 2014) that relatively small changes in the mean states can result in relatively
114 large changes in the behavior of ENSO. The set of seasonally varying mean fields required by LOAM are
115 the SST, near-surface winds, vertical structure of ocean temperature along the equator, upper ocean
116 currents and upwelling. To understand what can cause a change in the behavior of ENSO between two
117 climate states it is possible to use individual mean states from either climate to isolate, for example, the
118 impact of changing the mean wind. The governing equations in LOAM are provided in the Supplementary
119 Material (S.1), along with a summary of the constants and tuning parameters used in LOAM (Table S1;
120 Fig. S1).
121 Briefly, LOAM is comprised of a 1.5-layer ocean model and a two-layer atmosphere model in
122 which heating is a function of SST and surface wind convergence (Gill, 1980). The atmosphere is linear,
123 and modeled as a single baroclinic mode on an equatorial β-plane, with mechanical and thermodynamic
124 damping. In contrast to the (Zebiak and Cane, 1987) model and the (Battisti, 1988) model, the atmospheric
125 convergence feedback has been linearized as in (Battisti and Hirst, 1989). The ocean model consists of an
126 active upper layer, governed by the linear shallow water equations on an equatorial β-plane, and a
127 motionless lower layer. A 50 m deep Ekman layer, assumed to be in steady state with the surface winds, is
128 embedded in the active upper layer. The linearized prognostic equation for sea surface temperature (SST)
129 includes three-dimensional advection of temperature anomalies by the climatological currents, anomalous
130 advection of the climatological temperature, vertical mixing, and a simple parameterization of the surface
131 heat flux (Roberts and Battisti, 2011; Thompson, 1998b). The dependent variables for the ocean are:
132 meridional and zonal current, thermocline depth, and SST perturbations. The ocean equations are spectrally
133 discretized in the meridional direction by projecting them onto Rossby wave space, and discretized in the
134 zonal direction using finite differences. The atmosphere and SST equations are projected onto Hermite
135 functions in the meridional direction, and are discretized in the zonal direction using finite differences.
136 There are three parameters in LOAM that must be tuned using observations or model output,
137 which represent processes not resolved by the idealized model. These three tuning coefficients (one in the
138 atmosphere, two in the ocean) are described in the Supplementary Material. They are tuned independently

139 for the LOAM simulations with observed mean states and with CM2.1 mean states, as these two systems
140 are fundamentally different. However, the tuning parameters are held constant for all subsequent LOAM
141 experiments using the various CM2.1 mean states. In effect, we assume that these coefficients represent a
142 specific dynamical configuration of the system that is independent of the mean state changes across CM2.1
143 epochs. In this way, any changes in ENSO in the linearized model are due solely to changes in the mean
144 state fields and not to the tuning parameters.

145 Given a prescribed set of seasonally varying climatological mean fields (SST, near-surface winds,
146 vertical structure of ocean temperature along the equator, upper ocean currents and upwelling), LOAM
147 simulates the anomalies about the mean state. The underlying assumption in LOAM is that the dynamics of
148 the coupled system in the tropical Pacific are described by linear physics. The coupled atmosphere-ocean
149 variability in the tropical Pacific can then be characterized in terms of the stability, growth rate and
150 frequency of the system's Floquet modes (eigenmodes of the cyclo-stationary annual propagator matrix).
151 Because the eigenmodes of the coupled system are damped, the model is stochastically forced (as white
152 noise in space and time applied to the SST field). Thompson and Battisti (2001) and (Roberts and Battisti,
153 2011) demonstrated that LOAM with observed background states supports a leading mode of the coupled
154 system that has a similar spatial structure, decay rate, and period to that estimated from observations fit to
155 empirical models (Roberts and Battisti, 2011). The leading (slowest-decaying) Floquet mode in LOAM is
156 thus referred to as the ENSO mode. Given observed climatological mean states and white noise forcing,
157 LOAM produces reasonably realistic tropical Pacific climate variability, as demonstrated by the spatial
158 structure and variance explained by the leading EOFs of tropical Pacific SSTAs and the seasonal variance
159 and power spectra of SSTAs averaged over the Niño 3 region (5ºS-5ºN, 150ºW-90ºW; Roberts, 2007;
160 Roberts and Battisti, 2011). It has also been shown to capture the character of ENSO in GCMs, as well as
161 how ENSO can change in the presence of altered mean states (Roberts et al., 2014).

162 In the present study, we run LOAM with mean fields prescribed from each of three 40-year epochs
163 that were highlighted in Wittenberg (2009), Karamperidou et al. (2014), and Wittenberg et al. (2014),
164 characterized by low (Epoch L), medium (Epoch M) and high (Epoch H) ENSO variance in the CM2.1 pre-
165 industrial control simulation, and investigate the influence of the changes in tropical Pacific mean state on
166 ENSO. These runs are referred to as $\text{LOAM}_{\text{EPOCH L}}$, $\text{LOAM}_{\text{EPOCH M}}$ and $\text{LOAM}_{\text{EPOCH H}}$, respectively.

LOAM was also run with mean states prescribed to be the average over all three of these epochs, hereafter referred to as $LOAM_{CM2.1}$, as well as from observed mean fields, hereafter referred to as $LOAM_{OBS}$. In $LOAM_{OBS}$, the ocean temperature, currents, upwelling and wind stress fields are taken from the UMD Simple Ocean Data Assimilation reanalysis (SODA; Carton and Giese, 2008) for the period 1958–2001, and wind fields are taken from the European Centre for Medium-Range Weather Forecast ERA-40 reanalysis (http://apps.ecmwf.int/datasets/) for the same period. Stochastic forcing in LOAM is applied by adding a normally distributed random number to each of the spectrally and spatially discretized SST components in the model. The amplitude of the noise forcing is adjusted so that the variance of Niño 3 SST anomalies in LOAM equals that from observations, or from a given epoch of the CM2.1 control simulation. Specifically, three different estimates of the noise amplitude are used in the LOAM experiments: *(i)* F_M, in which the noise amplitude is adjusted so that the Niño 3 variance in LOAM is equal to that during Epoch M; *(ii)* $F_{CM2.1}$, in which the noise amplitude is adjusted so that the Niño 3 variance in LOAM is equal to that over the first 2000 years of the CM2.1 simulation; and *(iii)* F_{OBS}, in which the noise amplitude is adjusted so that the Niño 3 variance in LOAM is equal to that from the observed Niño 3 index. The SST output is smoothed with a 1-2-1 filter to reduce the noise, as in Zebiak and Cane (1987) and Thompson (1998). The various LOAM simulations implemented in this study are outlined in Table 1, along with their prescribed mean states and noise forcings.

3. Characteristics of tropical Pacific variability and extreme ENSO epochs in CM2.1

The GFDL CM2.1 global atmosphere/ocean/land/ice model has been widely recognized as a top-performing GCM with regard to its simulation of tropical climate variability, and featured prominently in the third Coupled Model Intercomparison Project (CMIP3) and the Intergovernmental Panel on Climate Change Fourth Assessment Report (Reichler and Kim, 2008; van Oldenborgh et al., 2005; Wittenberg et al., 2006). However, like most coupled GCMs, CM2.1 has biases in its ENSO simulation (Wittenberg et al., 2006). These include excessive ENSO variance (Fig. 5a,c; Fig. 7 (Takahashi and Dewitte, 2016; Wittenberg et al., 2006)) and biased spatial patterns of SST variability, including SST variability that extends too far west, is too equatorially-confined, and is underestimated in the far equatorial eastern Pacific

(Fig. 4a,c). Such ENSO biases are common in GCMs, and are likely tied to tropical Pacific mean state biases (Ham et al., 2013), which in CM2.1 include a cold SST bias along the equator, a warm bias along the coast of South America, and equatorial easterlies that are too broad zonally and extend too far into the western Pacific ((Wittenberg et al., 2006).

The 4,000 year-long pre-industrial control run of GFDL CM2.1 exhibits large variations in ENSO behavior on multi-decadal time scales, which have been the focus of a number of recent studies (Karamperidou et al., 2014; Wittenberg, 2009; Wittenberg et al., 2014). In the control run of this model, the variance of Niño 3 SSTAs during a given 40-year epoch can vary by over a factor of four (from 0.7 – 3.0 $°C^2$; Fig. 1). In this paper we focus on three 40-year periods in the CM2.1 control run that were highlighted in (Wittenberg, 2009), (Karamperidou et al., 2014), and (Wittenberg et al., 2014), to represent the diversity of the model's ENSO variability. The time series of Niño 3 SSTAs for each period are shown in Fig. 1b-d. Years 1151 – 1190 (Epoch L) represent a period of extreme low variability (variance of Niño 3 SSTAs = 0.7 $°C^2$). Years 531-570 (Epoch M) are characterized by variability that is similar to the mean of the first 2,000 years (variance of Niño 3 SSTAs = 1.8 $°C^2$), with fairly normally-distributed Niño 3 SSTAs that have a regular periodicity. Years 1711-1750 (Epoch H) are characterized by numerous intense warm events (variance of Niño 3 SSTAs = 3.0 $°C^2$) that are farther apart in time and have less regular periodicity than those in Epoch M.

The leading patterns of tropical Pacific SST variability in each epoch are shown in Fig. 2. Empirical orthogonal functions (EOFs) 1-3 display roughly similar characteristics across epochs. Notably, a lower fraction of the total variance is explained by the first two EOFs in Epoch L relative to the other epochs and EOFs 2 and 3 appear to be mixed in Epoch M (their eigenvalues are not distinguishable). Fig. 3 shows that compared to the long-term variance, the region of maximum variance in Epoch L is reduced and shifted east, while that in Epoch H is amplified and shifted west.

4. ENSO in a linearized intermediate model versus GFDL CM2.1

As part of our analysis to investigate the sources of the low-frequency ENSO modulation in CM2.1, we employ a linearized anomaly model of the tropical Pacific (LOAM). The rationale for this

223 approach is that it has been shown that all but the strongest observed ENSO events are well represented by
224 linear dynamics (Penland and Sardeshmukh, 1995; Roberts and Battisti, 2011). Furthermore, comparison of
225 the linear model simulations to the fully nonlinear CM2.1 simulation enables a rough partitioning of the
226 linear and nonlinear components of ENSO evolution in CM2.1.

227 The LOAM simulation with mean fields prescribed from the CM2.1 climatology averaged over all
228 120 years of the three epochs ($LOAM_{CM2.1}$), demonstrates spatial and temporal patterns of tropical Pacific
229 SSTA variability that compare well in some aspects to CM2.1, while other features are notably dissimilar
230 (Figs. 4-7). Differences include the region of maximum variance, which does not extend as far west in
231 $LOAM_{CM2.1}$ and is broader meridionally and weaker near the eastern boundary than in CM2.1 (c.f. Fig.
232 4c,d). In addition, Niño 3 SSTAs in CM2.1 display large asymmetry in the amplitude of warm versus cold
233 events (Fig. 5c; Fig. 6), indicating the presence of strong nonlinearities in CM2.1 (Choi et al., 2013 2015).
234 In contrast, Niño 3 SSTAs in LOAM are linear by construction (Fig. 5d, Fig. 6). The power spectrum of
235 the first 2,000 years of Niño 3 SSTAs in CM2.1, much like the observations, shows a broad spectral peak
236 between 2-5 yr (median period 3.4 yr), while the power spectrum in $LOAM_{CM2.1}$ is much more sharply
237 peaked (median period 3.2 yr; Fig. 7). These results suggest that ENSO nonlinearities and/or multiplicative
238 noise, which are not included in LOAM, may be important contributors to the temporal and spatial
239 structure of ENSO in CM2.1.

240 In nature, ENSO is strongly synchronized to the calendar year, with ENSO events tending to peak
241 in boreal winter (Fig. 8a). In contrast, ENSO in CM2.1 displays weak seasonality, with Niño 3 SSTA
242 variance peaking in boreal summer (Fig. 8c). Given CM2.1 mean states, ENSO in LOAM displays a
243 notably distinct seasonality from CM2.1, with variance reaching a minimum in May/June and peaking
244 around Sept. (Fig. 8d). The differences in seasonality between $LOAM_{CM2.1}$ and LOAM tuned to
245 observations ($LOAM_{OBS}$, panels b and d in Fig. 8) are likely related to the biased annual cycle in CM2.1,
246 through its influence on the seasonal growth rate of ENSO. In particular, the CM2.1 climatological wind
247 field features an overly muted and delayed relaxation of the trades during boreal spring and an
248 enhancement of the trades during boreal summer and fall that is too strong and does not persist into the
249 winter. The trade wind biases are associated with a stronger semi-annual cycle in the tropical Pacific than is
250 observed (Wittenberg, 2009).

These results indicate that LOAM is able to capture some, but not all of the important features of ENSO behavior in CM2.1. Shortcomings of LOAM include the absence of surface heat flux dependence on wind speed (which may account for the difference in SST variability in the western Pacific and in the subtropics in CM2.1 versus LOAM; c.f. Fig. 4c,d). In addition, LOAM omits all nonlinear dynamics, including nonlinear dependence of atmospheric heating and wind stress anomalies on SST anomalies and nonlinear ocean dynamics (Chen et al., 2016; Choi et al., 2013; Takahashi and Dewitte, 2016). However, that LOAM has successfully managed to capture many of the fundamental characteristics of observed ENSO (Roberts and Battisti, 2011; Thompson and Battisti, 2001) as well as capture changes to ENSO from mean state changes in other CGCMs (Roberts et al., 2014) suggests that the inability of LOAM to characterize some of the important features of ENSO in CM2.1 is because CM2.1's ENSO does not conform to the assumptions that are in LOAM, e.g. due to the strong nonlinearities in CM2.1.

Given the success of LOAM in simulating many observed features of ENSO variability, the linear model provides an excellent opportunity to contrast the linear components of ENSO evolution with the full nonlinear evolution in CM2.1. It also allows investigation of how the mean state contributes to the (linear component of the) differences in variance between the L, M, and H epochs. We thus use LOAM to evaluate the linear component of the ENSO dynamics, sensitivities, and feedbacks in CM2.1. While this linear component is dominant in observations, it appears to be less so in CM2.1. The misfit of LOAM's ENSO to CM2.1's ENSO is then one measure of the importance of nonlinearities in CM2.1.

5. Drivers of low frequency ENSO modulation in CM2.1

Because the CM2.1 control simulation is unforced, there are essentially four, non mutually exclusive, mechanisms that could cause the large multi-decadal ENSO variability: (1) low frequency changes in the tropical Pacific mean state, which alter the stability of the ENSO system; (2) low frequency changes in stochastic (weather) processes that influence ENSO; (3) random sampling from a stationary, linear process; and (4) nonlinear dynamics, including multiplicative noise, in the ENSO system that spreads variance over a range of time scales-- e.g. nonlinear interaction between the annual cycle and internal

modes of variability in the tropical Pacific that produce deterministic chaos (see e.g. Timmermann et al., 2002). We discuss each of these possible mechanisms, below:

i. Influence of tropical Pacific mean state changes on ENSO in the linear model

In their examination of the multi-decadal rectification of ENSO modulation in CM2.1, Ogata et al. (2013) demonstrated that mean state changes during the different CM2.1 epochs may be generated by the extreme ENSO behavior (that is, they are the residual impact of the ENSO cycles during each epoch), as also suggested by (Vimont, 2005), (Wittenberg, 2009), and (Wittenberg et al., 2014). The concept that ENSO is highly sensitive to mean state changes in the tropical Pacific has been widely explored and demonstrated, typically in studies that invoke intermediate complexity models of varying descriptions (Battisti and Hirst, 1989; Dewitte, 2000; Roberts et al., 2014; Wittenberg, 2002; Zebiak and Cane, 1987). It has further been suggested that the post-1970's shift in ENSO characteristics may be related to changes in the tropical Pacific background state (An and Wang, 2000).

We sought to evaluate the impacts of the tropical Pacific mean state changes in CM2.1 on ENSO by prescribing the annual cycle of tropical Pacific climatology averaged separately over the three representative CM2.1 epochs in LOAM. The differences in annually-averaged tropical Pacific climatology among these epochs are shown in Figs. 9 and 10. Progressing from Epoch L to Epoch H, the mean states are characterized by weakening of the surface easterly trade winds in the western and central equatorial Pacific, warming of the ocean surface and subsurface in the eastern equatorial Pacific, and cooling in the western equatorial Pacific (Fig. 9; Fig. 10) -- consistent with the results of Ogata et al. (2013) in their examination of the multi-decadal rectification of ENSO modulation in CM2.1.

When the mean states from the three CM2.1 epochs are prescribed in LOAM, the relative changes in the variance of Niño 3 SSTAs in the linear model are *opposite* to those observed in the CM2.1 simulation: the variance is lowest in Epoch H and highest in Epoch L (Table 1; Fig. 11). In Epoch H, the decreased ENSO variance relative to Epoch M is due to a decrease in the growth rate of the ENSO mode. In Epoch L, the increase in variance relative to Epoch M is tied to the increased growth rate of the lower order coupled modes (not shown). Collectively, our results lend support to the idea that tropical Pacific

mean state changes are not the primary cause of the intrinsically-generated extreme ENSO epochs in the CM2.1 control run.

That the LOAM simulations demonstrate the sensitivity of the linear component of ENSO to changes in the tropical Pacific mean state (Table 1), is suggestive of a two-way feedback mechanism between low frequency ENSO modulation and tropical Pacific mean state changes in CM2.1, wherein: (1) stochastic forcing and nonlinearity produce low frequency ENSO modulation, which rectify into tropical Pacific mean state changes due to the ENSO asymmetries in CM2.1; (2) these rectified mean state changes then feed back negatively on the ENSO growth rates, thus tempering the ENSO modulation. For example, as shown in Ogata et al. (2013), strong-ENSO epochs in CM2.1 weaken the multi-decadal zonal SST gradient and zonal winds in the central to western equatorial Pacific (Fig 9c), and thus weaken the zonal tilt of the thermocline (Fig 10b). According to the stability analysis performed with LOAM, these mean state changes act to stabilize the coupled system and weaken ENSO (Table 1). Along the same lines, weak-ENSO epochs in CM2.1 strengthen the multi-decadal zonal SST gradient and zonal wind stress in the central to western equatorial Pacific (Fig. 9B), and thus strengthen the zonal tilt of the thermocline (Fig. 10A). The LOAM stability analysis indicates that these mean state changes act to destabilize the lower order modes (not shown) and thereby modestly strengthen the ENSO variability (Table 1; Fig. 11).

Further experiments were performed with LOAM, in which individual components of the mean states of Epochs H and L were substituted into the Epoch M simulation. Results from these experiments (not shown) indicate two primary mechanisms of increased stability of the coupled system in Epoch H. First, the weaker climatological trade winds lead to reduced coupling via the linear dependence of the wind stress anomalies on the mean wind speed in LOAM (see Eqn. 18 in Supplemental Material; (see Eqn. 18 in Supplemental Material; Battisti and Hirst, 1989). Second, a weaker mean zonal tilt of the equatorial thermocline leads to weaker contribution of anomalous upwelling to SST changes (i.e. weakened upwelling feedback; see Eqns. 1-3 in the Supplementary Material). Details of these feedback processes can be found in (Thompson, 1998a, b) and (Roberts and Battisti, 2011). The primary mechanisms of *decreased* stability of the coupled system in Epoch L are the same as those discussed above, only with opposite sign (e.g. stronger climatological winds enhance coupling).

There are two caveats to the proposed negative feedback mechanism between the tropical Pacific mean state changes and low frequency ENSO modulation in CM2.1. First, nonlinearities in CM2.1 may act to compensate for these large "mean state induced" changes in the linear stability, thereby tempering the sensitivity of ENSO to mean state changes. Second, because LOAM does not include state-dependent noise forcing, any influence that the mean state changes may have on the noise forcing are not considered in this analysis.

ii. Influence of changes in atmospheric noise on low-frequency ENSO modulation

The results highlighted in the previous section suggest that mean state changes in the tropical Pacific do not explain the periods of extreme ENSO variability in CM2.1 -- suggesting that the ENSO modulation in CM2.1 is instead driven by atmospheric noise and/or nonlinear dynamics. These results are consistent with the results presented in (Wittenberg et al., 2014), who showed that the occurrence of extreme-ENSO epochs in CM2.1 were in fact unpredictable.

Multi-decadal fluctuations of ENSO variability could arise through low frequency changes in the structure and/or amplitude of the atmospheric noise forcing (either internal or external to the tropical Pacific), including a multiplicative dependence of westerly wind bursts on the zonal extent of the Pacific warm pool (Graham et al., 2016). While an attempt was made to characterize the noise forcing in the three CM2.1 epochs using a Linear Inverse Model (LIM; e.g. Penland and Sardeshmukh, 1995), it was concluded that 40 years of CM2.1 data was not long enough to robustly constrain the dynamics of the coupled system (see S.2 in the Supplemental Material for details). These results are in contrast to those from (Newman et al., 2011), in which 42 years was deemed sufficient to constrain a LIM trained on observational data. These results again highlight the difference between ENSO in CM2.1 and ENSO in nature -- the LIM fit to CM2.1's strongly-modulated ENSO system is less robust to short epochs than the LIM fit to observations. Because of these issues, the possible role of changes in atmospheric noise forcing on CM2.1's ENSO modulation has yet to be evaluated.

iii. Low-frequency ENSO modulation through randomly sampling a stationary, linear process

359 Independent from any changes in the background climate state or the structure or amplitude of
360 atmospheric noise forcing, multi-decadal variations in ENSO variability arise solely due to random
361 sampling from a system governed by linear, stationary dynamics. For a stationary, linear process with well-
362 defined long-term variance, and for epochs that randomly and independently sample the underlying
363 distribution of multi-decadal ENSO variance, the probability distribution function (PDF) of epochal
364 variance will match that of a χ^2 distribution (Russon et al., 2014).
365 In order to compare a χ^2 distribution to the ENSO modulation present in CM2.1, the probability
366 distribution of ENSO variance (hereafter defined as the variance of Niño 3 SSTAs) in 40-year intervals was
367 plotted from the first 2,000 years of the CM2.1 simulation alongside χ^2 distributions (Fig. 12), calculated
368 using Eqns. 1-2, below (from Russon et al., 2014). To further compare CM2.1's ENSO modulation with
369 that of a linear system with additive noise, the 2,000-year LOAM simulation with CM2.1 mean states and
370 CM2.1-tuned noise, and the 2,000-year LOAM simulation with observed mean states and observation-
371 tuned noise were also plotted.
372 While one might expect the temporal properties of ENSO in the low-dimensional, linear system in
373 LOAM to be notably distinct from the high dimensional, fully nonlinear CM2.1, the distribution of multi-
374 decadal ENSO variance is notably similar in CM2.1 and the linear model, with the exception of a slightly
375 broader distribution in CM2.1. A two-sample Kolmogorov-Smirnov test of the variance histograms
376 indicates that the null hypothesis (that the two data sets were drawn from the same distribution) cannot be
377 rejected. The correspondence of the CM2.1 histogram with the χ^2 distribution indicates that ENSO statistics
378 even in the highly nonlinear CM2.1 are roughly stationary at multi-decadal time scales. This result is
379 consistent with the finding by (Wittenberg, 2009) and (Wittenberg et al., 2014) who showed that the warm
380 events in CM2.1 resembled a memory-less interannual process with no decadal-scale predictability. These
381 findings demonstrate that the low-frequency ENSO modulation in CM2.1 is driven by transient processes
382 that operate at time scales that are interannual or shorter.
383 Like most coupled GCMs, CM2.1 has biases in its ENSO simulation (Wittenberg et al., 2006).
384 Importantly, these biases include excessive ENSO variance in CM2.1 (Fig. 5a,c; Fig. 7 (Takahashi and
385 Dewitte, 2016; Wittenberg et al., 2006)). In order evaluate the influence of this overly strong ENSO
386 variance on the low-frequency ENSO modulation, the variance distribution from the LOAM simulation

tuned to observations ($LOAM_{OBS} + F_{OBS}$; red histogram in Fig. 12) was compared to the distribution from the LOAM simulation tuned to CM2.1 ($LOAM_{CM2.1} + F_{CM2.1}$; black histogram in Fig. 12). The results demonstrate that the distribution with weaker ENSO variance ($LOAM_{OBS} + F_{OBS}$) is much more sharply peaked about its respective mean than the distribution with stronger ENSO variance ($LOAM_{CM2.1} + F_{CM2.1}$). Indeed, the range of multi-decadal variance in CM2.1 (and LOAM tuned to CM2.1) is twice that produced by LOAM tuned to observations.

There is a simple statistical reason for this, which explains how CM2.1's strong ENSO variance is directly related to its strong inter-epoch modulation of ENSO variance (Fig. 12). Given a normal distribution with variance σ^2, the expected distribution of the sample variance of a random sample of size n is

$$s^2 = \frac{\sigma^2 \chi^2_{n^*-1}}{n^* - 1} \qquad (1)$$

where χ^2_{n-1} is the Chi-square distribution with n-1 degrees of freedom. n^* can be estimated from:

$$n^* = \frac{n}{\tau_d}; \quad \tau_d = 1 + \sum_{i=1}^{L} {\rho_i}^2 \qquad (2)$$

where τ_d is a dimensionless factor by which the effective degrees of freedom are reduced relative to the number of data points in each interval (here, 480) and is constrained by the autocorrelation of the Nino 3 SSTA data. The autocorrelation function (ρ) is summed over the number of time steps (L) needed to reach the first two sign changes in the autocorrelation function (von Storch and Zwiers, 2003; Russon et al., 2014). Now suppose that ENSO is memoryless beyond a few years -- as in CM2.1, in which the wait times between El Niño events are Poisson-distributed at decadal and longer scales (Wittenberg, 2009), with no apparent decadal predictability of ENSO amplitude (Wittenberg et al., 2014). Further suppose that the Niño 3 SST anomalies have long-term variance σ^2, and that each 40-year epoch contains n effectively-independent samples of the Niño 3 SST anomalies. The inter-epoch spread of the epochal variance, i.e. the variance modulation, would then increase like the square of the long-term variance σ^2:

$$\mathrm{Var}(s^2) = \left(\frac{\sigma^2}{n-1}\right)^2 \mathrm{Var}(\chi^2_{n-1}) = \left(\frac{\sigma^2}{n-1}\right)^2 2(n-1) = \frac{2\sigma^4}{(n-1)} \qquad (3)$$

In simple terms, a weak memoryless ENSO can only exhibit weak variance, while a strong memoryless ENSO can exhibit either strong or weak variance – resulting in much more variance modulation. This

disparity is largely removed if the relative change in variance (with respect to the long-term variance) is compared instead (Fig. 12b). In this case the empirical distributions are highly similar, and thus a -40 to + 55% change in ENSO variance in a given 40-year interval (representing 2.5-97.5% of the CM2.1 distribution) is similarly likely in the CM2.1, $LOAM_{CM2.1}$ and $LOAM_{OBS}$ simulations.

To summarize: these results indicate that the distribution of ENSO variance in CM2.1 is dramatically broadened with respect to the linear system with ENSO variance tuned to that observed over the past 50 years. However, the broad CM2.1 distribution is entirely consistent with the distribution expected from a linear system that has excessive ENSO variance. The correspondence of the CM2.1 histogram with that from the linear model and the χ^2 distribution indicates that ENSO statistics in CM2.1 are roughly stationary at multi-decadal time scales, demonstrating that the low-frequency ENSO modulation in CM2.1 is driven by transient processes that operate at time scales that are interannual or shorter. Taken together, the results from the linear LOAM and nonlinear CM2.1 show that a memory-less interannual ENSO, whether linear or highly nonlinear, will generate interdecadal variance modulation that resembles a χ^2 distribution, and that the variance modulation increases sharply as ENSO strengthens. In this way, CM2.1's overly strong ENSO variance directly contributes to its strong multi-decadal modulation. In absolute terms, the multi-decadal modulation in CM2.1 is twice that produced by a linear system tuned to the ENSO variance observed over the past 50 years. In contrast, the relative changes in ENSO modulation are notably similar between the linear and nonlinear models, with the exception of a slightly broader distribution in the nonlinear CM2.1. These results underscore the findings of Russon et al. (2014) that only relative changes in multi-decadal ENSO variance can robustly be compared across models and observations.

(iv) The influence of nonlinearities on low-frequency ENSO modulation in CM2.1

While the results presented in Section *(iii)* demonstrate that the nonlinearities in CM2.1 do not dramatically broaden the distribution of variance *as compared to a linear system with equal ENSO variability*, this does not imply that nonlinearities are entirely unimportant in determining the multi-decadal modulation of ENSO. The nonlinearities may in fact be critical to the multi-decadal ENSO modulation by contributing to the overly active ENSO variability that causes the enhanced multi-decadal modulation, e.g.

through enhancing the growth of strong El Nino events (e.g. Takahashi and Dewitte, 2016).[1] Additional simulations with LOAM suggest that linear dynamics operating on the biased CM2.1 mean states are *not* the source of the overactive ENSO activity in CM2.1 (see S.3 in the Supplementary Material) -- which in turn further suggests that nonlinear dynamics and multiplicative noise likely play an important role in driving the excessive ENSO variance, and thus low-frequency ENSO modulation, present in CM2.1. Results presented below indeed demonstrate that these nonlinearities are inextricably linked to the low-frequency ENSO modulation in CM2.1.

The coupled ocean-atmosphere system appears to be substantially more nonlinear in CM2.1 than has been observed over the past 50 years (Fig. 13-14). A key nonlinearity in CM2.1 is the response of the central Pacific low-level wind (and zonal wind stress) anomalies to SST anomalies– indicative of the Bjerknes feedback that is central to the physics of ENSO (Battisti and Hirst, 1989). This feedback is approximately linear for all but the strongest El Nino events in the observations, while a highly nonlinear feedback is present in CM2.1 (Fig. 13; Fig. S2). These results suggest that the highly nonlinear response of the atmosphere to central Pacific SST anomalies may be responsible for the growth of strong El Nino events in CM2.1.

Previous studies have also suggested that the key nonlinearities relevant to ENSO in CM2.1 are in the atmosphere (Chen et al., 2016; Choi et al., 2013; Takahashi and Dewitte, 2016). Possible sources of the nonlinear response of the atmosphere to SST anomalies in CM2.1 may include a nonlinear moisture convergence feedback, changes in the character of the central Pacific atmospheric boundary layer associated with shifts in the edge of the warm pool convective region, the nonlinear relationship between specific humidity and surface air temperature in the tropics, and state-dependent multiplicative noise forcing (see S.4 in the Supplementary Material for further discussion; (e.g. the eastward shift of westerly wind events, as the warm pool shifts eastward during the onset of El Nino events; Graham et al., 2016;

[1] However, it is also possible that the strong nonlinearity in CM2.1 is a symptom, rather than a cause of its strong ENSO variability. The strong climatological cold tongue in CM2.1 suggests that the model has overactive ocean-dynamical cooling. If this is indeed the case, hyperactive (but possibly still linear) subsurface ENSO feedbacks may be the driver of its higher amplitude SSTAs. In a model with a climatological equatorial cold bias (which shifts the atmospheric convective zones farther to the west and farther off-equator), those greater SSTAs then produce a greater atmospheric nonlinearity Choi, K.Y., Vecchi, G.A., Wittenberg, A.T., 2013. ENSO Transition, Duration, and Amplitude Asymmetries: Role of the Nonlinear Wind Stress Coupling in a Conceptual Model. Journal of Climate 26, 9462-9476..

Levine, in press; Vecchi et al., 2006). Each of these nonlinearities may be amplified by the background state biases in the Pacific of CM2.1, including an excessive contrast between the off-equatorial convergence zones (which are too rainy) and the eastern equatorial cold tongue (over which the atmosphere is too clear and dry). This enhanced contrast could strengthen the atmospheric nonlinearity near the equator, by giving convection more room to increase during El Nino and less room to decrease during La Niña (Chen et al., 2016). Whatever the source(s) of the overly nonlinear Bjerknes feedback in the central Pacific in CM2.1, it appears to give rise to larger ENSO events than those yet observed.

Evidence for an important role of such transient nonlinearities in driving the low-frequency ENSO modulation in CM2.1 can be seen by evaluating the SST and wind/windstress anomalies separately for the high- and low-variance ENSO epochs. High-variance ENSO epochs in CM2.1 are populated by more extreme ENSO events (panels A and B of Fig. 13), which are governed by a highly nonlinear Bjerknes feedback in the central Pacific. The threshold behavior of zonal wind and wind stress anomalies in the central Pacific during these epochs in response to warm SST anomalies are evidence of this strong nonlinearity (Fig. 13b; Fig. 14b; as identified in Takahashi and Dewitte, 2016), as is the large positive skewness in central Pacific wind stress anomalies (Fig. 14D) and in eastern Pacific SST anomalies (Fig. 15D). In contrast, the low-variance epochs are characterized by weaker ENSO events with more linear behavior (Fig. 13A,B; panel C of Fig. 14 and 16). From these results we conclude that (1) the physics of the coupled ocean-atmosphere system in CM2.1 are close to linear for the weaker ENSO epochs, resembling the past 50 years; and (2) CM2.1's high-variance ENSO epochs (such as Epoch H; Fig. 1D) are generated by a collection of stochastically-driven extreme ENSO events that are highly nonlinear. From these analyses we conclude that transient nonlinearities or multiplicative noise help drive the low-frequency ENSO modulation in CM2.1. This is consistent with previous results showing that CM2.1's ENSO modulation is decadally unpredictable (Wittenberg et al., 2014) and produces rectified effects on the decadal mean state (Ogata et al., 2013).

6. Conclusions

Large, unforced, multi-decadal changes in ENSO variability have been previously reported from the long pre-industrial control run of GFDL CM2.1. We evaluated the possible sources of this low-

492 frequency ENSO modulation, by characterizing the extreme ENSO epochs in CM2.1 and employing a
493 linearized intermediate-complexity model of the tropical Pacific (LOAM).

494 Simulations with the linear model demonstrate that intrinsically-generated tropical Pacific decadal
495 mean state changes produced through a rectified nonlinear response to the low frequency ENSO
496 modulation do not contribute to the extreme-ENSO epochs in CM2.1. Rather, these decadal mean state
497 changes actually serve to *damp* the ENSO modulation, primarily by stabilizing the ENSO mode during
498 strong-ENSO epochs. These results point to a possible feedback loop between ENSO and the mean state --
499 whereby noise and nonlinearities produce extreme ENSO epochs, which are then counteracted by linear
500 feedbacks from the mean state. However, it is also possible that in CM2.1, nonlinearities and/or state-
501 dependent noise forcing give rise to mean state feedbacks that are not predicted by the linear model.

502 The presence of low frequency changes in stochastic (weather) processes is difficult to address
503 using the suite of tools employed in this analysis and thus its contribution to the low-frequency ENSO
504 modulation in CM2.1 has yet to be evaluated. However, we demonstrate (using the linear model runs,
505 CM2.1, and observations) that the low-frequency ENSO modulation can be well described by the simplest
506 model of a linear, stationary process. These results indicate that even in the highly nonlinear CM2.1, ENSO
507 statistics are roughly stationary at multi-decadal time scales (in the absence of external forcings); and the
508 intrinsic low-frequency ENSO modulation in CM2.1 is driven by transient processes operating at
509 interannual or shorter time scales. One might expect nonlinearities, multiplicative noise, and other physics
510 not included in the simple linear model to contribute significantly to the spectral broadening of ENSO, in
511 both the observations and CM2.1. However, we show that their effects on the level of ENSO modulation
512 appear to be weak, compared to the effects of the strong ENSO variance in CM2.1.

513 We demonstrate that nonlinearities are inextricably linked to the multi-decadal ENSO modulation
514 in CM2.1. High-variance ENSO epochs in CM2.1 are populated by extreme ENSO events that are
515 characterized by a highly nonlinear Bjerknes feedback in the central Pacific; low-variance epochs are
516 characterized by weaker ENSO events with more linear behavior. While nonlinearities in CM2.1 do not
517 dramatically broaden the distribution of variance compared to a linear system with equal long-term ENSO
518 variance, the nonlinearities likely shape the amplitude distribution of ENSO modulation by contributing to

519 an overactive ENSO (e.g. by intensifying strong El Nino events), which then broadens the distribution of
520 epochal ENSO variance.

521 These results have important implications for understanding the past, present, and future of ENSO.
522 Taken at face value, CM2.1's strong unforced decadal-to-centennial modulation of ENSO would suggest
523 that existing observational records might be too short to rule out such modulation in the real world (e.g. a
524 factor of four spread in the variance of Niño 3 SSTAs during different 40-year epochs). Therefore, to detect
525 a *forced* change in ENSO variability, e.g. using proxy recorders like Pacific corals to characterize the pre-
526 instrumental epoch, either the records would have to be long or the change large. However, our results
527 suggest that if the past 50 years of observations are representative of the average interannual variance of
528 ENSO in the real world, then the true spectrum of unforced ENSO modulation is, in absolute terms, likely
529 substantially narrower than that suggested by CM2.1. Forced changes might therefore be detectable using
530 relatively short records. However, when *relative*, rather than absolute, changes in ENSO variance are
531 compared, the distributions of variance are remarkably insensitive to the differing ENSO characteristics.
532 The statistics of the *relative* changes in ENSO variance might therefore be extrapolated from the fully
533 nonlinear CM2.1 to other systems (e.g. those with less variable and/or more linear ENSOs).

534 Lastly, we note that tropical Pacific mean state changes due to future greenhouse gas increases are
535 projected to grow substantially larger than the unforced mean state changes seen between the weak-ENSO
536 versus strong-ENSO epochs in CM2.1 (Wittenberg, 2015; Xie et al., 2010). Given projected future climate
537 changes in the tropical Pacific, the LOAM-inferred ENSO sensitivity would suggest substantial and
538 detectable changes in ENSO that are consistent with actual forced CM2.1 scenarios (Wittenberg, 2015). On
539 the other hand, the LOAM-inferred ENSO sensitivity would also suggest that the mean state *biases*
540 prevalent in GCMs could have large impacts on how ENSO responds to forcings -- underscoring the
541 critical need to reduce these biases, in order to make reliable projections of the future of ENSO.

References

An, S.-I., Wang, B., 2000. Interdecadal change of the structure of the ENSO mode and its impact on the ENSO frequency. Journal of Climate 13, 2044-2055.

Battisti, D.S., 1988. Dynamics and thermodynamics of a warming event in a coupled tropical atmosphere-ocean model. Journal of the Atmospheric Sciences 45, 2889-2919.

Battisti, D.S., Hirst, A.C., 1989. Interannual variability in a tropical atmosphere ocean model- influence of the basic state, ocean geometry and nonlinearity. Journal of the Atmospheric Sciences 46, 1687-1712.

Bellenger, H., Guilyardi, E., Leloup, J., Lengaigne, M., Vialard, J., 2014. ENSO representation in climate models: from CMIP3 to CMIP5. Climate Dynamics 42, 1999-2018.

Cai, W.J., Borlace, S., Lengaigne, M., van Rensch, P., Collins, M., Vecchi, G., Timmermann, A., Santoso, A., McPhaden, M.J., Wu, L.X., England, M.H., Wang, G.J., Guilyardi, E., Jin, F.F., 2014. Increasing frequency of extreme El Nino events due to greenhouse warming. Nature Climate Change 4, 111-116.

Capotondi, A., Ham, Y.-G., Wittenberg, A.T., Kug, J.-S., 2015. Climate model biases and El Niño Southern Oscillation (ENSO) simulation. U.S. CLIVAR Variations 13, 21-25.

Carton, J.A., Giese, B.S., 2008. A reanalysis of ocean climate using Simple Ocean Data Assimilation (SODA). Monthly Weather Review 136, 2999-3017.

Chen, C., Cane, M.A., Wittenberg, A.T., Chen, D., 2016. ENSO in the CMIP5 simulations: Lifecycles, diversity, and responses to climate change. Journal of Climate in press.

Choi, K.Y., Vecchi, G.A., Wittenberg, A.T., 2013. ENSO Transition, Duration, and Amplitude Asymmetries: Role of the Nonlinear Wind Stress Coupling in a Conceptual Model. Journal of Climate 26, 9462-9476.

Cobb, K.M., Westphal, N., Sayani, H.R., Watson, J.T., Di Lorenzo, E., Cheng, H., Edwards, R.L., Charles, C.D., 2013. Highly Variable El Nino-Southern Oscillation Throughout the Holocene. Science 339, 67-70.

568 Collins, M., An, S.I., Cai, W.J., Ganachaud, A., Guilyardi, E., Jin, F.F., Jochum, M., Lengaigne, M.,
569 Power, S., Timmermann, A., Vecchi, G., Wittenberg, A., 2010. The impact of global warming on
570 the tropical Pacific ocean and El Nino. Nature Geoscience 3, 391-397.
571 Delworth, T.L., Broccoli, A.J., Rosati, A., Stouffer, R.J., Balaji, V., Beesley, J.A., Cooke, W.F., Dixon,
572 K.W., Dunne, J., Dunne, K.A., Durachta, J.W., Findell, K.L., Ginoux, P., Gnanadesikan, A.,
573 Gordon, C.T., Griffies, S.M., Gudgel, R., Harrison, M.J., Held, I.M., Hemler, R.S., Horowitz,
574 L.W., Klein, S.A., Knutson, T.R., Kushner, P.J., Langenhorst, A.R., Lee, H.C., Lin, S.J., Lu, J.,
575 Malyshev, S.L., Milly, P.C.D., Ramaswamy, V., Russell, J., Schwarzkopf, M.D., Shevliakova, E.,
576 Sirutis, J.J., Spelman, M.J., Stern, W.F., Winton, M., Wittenberg, A.T., Wyman, B., Zeng, F.,
577 Zhang, R., 2006. GFDL's CM2 global coupled climate models. Part I: Formulation and simulation
578 characteristics. Journal of Climate 19, 643-674.
579 Dewitte, R., 2000. Sensitivity of an intermediate ocean-atmosphere coupled model of the tropical Pacific to
580 its oceanic vertical structure. Journal of Climate 13, 2363-2388.
581 DiNezio, P.N., Kirtman, B.P., Clement, A.C., Lee, S.K., Vecchi, G.A., Wittenberg, A., 2012. Mean
582 Climate Controls on the Simulated Response of ENSO to Increasing Greenhouse Gases. Journal of
583 Climate 25, 7399-7420.
584 Gill, A.E., 1980. Some simple solutions for heat-induced tropical circulation. Quarterly Journal of the
585 Royal Meteorological Society 106, 447-462.
586 Graham, F.S., Wittenberg, A.T., Brown, J.N., Marsland, S.J., Holbrook, N.J., 2016. Understanding the
587 double peaked El Niño in coupled GCMs. Climate Dynamics in press.
588 Guilyardi, E., Bellenger, H., Collins, M., Ferrett, S., Cai, W., Wittenberg, A., 2012a. A first look at ENSO
589 in CMIP5. Clivar Exchanges 58, 29-32.
590 Guilyardi, E., Cai, W.J., Collins, M., Fedorov, A., Jin, F.F., Kumar, A., Sun, D.Z., Wittenberg, A., 2012b.
591 New strategies for evaluating ENSO processes in climate models. Bulletin of the American
592 Meteorological Society 93, 235-238.
593 Guilyardi, E., Wittenberg, A., Fedorov, A., Collins, M., Wang, C., Capotondi, A., van Oldenborgh, J.,
594 Stockdale, T., 2009. Understanding El Nino in Ocean-Atmosphere General Circulation Models.
595 Bulletin of the American Meteorological Society 90, 325-340.

596 Guilyardi, E.W., A.; Balmaseda, M.; Cai, W.; Collins, M.; McPhaden, M.; Watanabe, M.; Yeh, S.-W., in
597 press. ENSO in a changing climate: Meeting summary of the 4th CLIVAR workshop on the
598 evaluation of ENSO processes in climate models. Bull. Am. Meteorol. Soc.
599 Ham, Y.G., Kug, J.S., Kim, D., Kim, Y.H., Kim, D.H., 2013. What controls phase-locking of ENSO to
600 boreal winter in coupled GCMs? Climate Dynamics 40, 1551-1568.
601 Karamperidou, C., Cane, M.A., Lall, U., Wittenberg, A.T., 2014. Intrinsic modulation of ENSO
602 predictability viewed through a local Lyapunov lens. Climate Dynamics 42, 253-270.
603 Koutavas, A., Demenocal, P.B., Olive, G.C., Lynch-Stieglitz, J., 2006. Mid-Holocene El Nino-Southern
604 Oscillation (ENSO) attenuation revealed by individual foraminifera in eastern tropical Pacific
605 sediments. Geology 34, 993-996.
606 Kug, J.S., Choi, J., An, S.I., Jin, F.F., Wittenberg, A.T., 2010. Warm Pool and Cold Tongue El Nino Events
607 as Simulated by the GFDL 2.1 Coupled GCM. J. Clim. 23, 1226-1239.
608 Levine, A.F.Z.J., F. F, in press. A simple approach to quantifying the noise-ENSO interaction. Part 1:
609 deducing the state-dependency of the windstress forcing using monthly mean data. Clim. Dyn.
610 McGregor, H.V., Fischer, M.J., Gagan, M.K., Fink, D., Phipps, S.J., Wong, H., Woodroffe, C.D., 2013. A
611 weak El Nino/Southern Oscillation with delayed seasonal growth around 4,300 years ago. Nature
612 Geoscience 6, 949-953.
613 Newman, M., Alexander, M.A., Scott, J.D., 2011. An empirical model of tropical ocean dynamics. Clim.
614 Dyn. 37, 1823-1841.
615 Ogata, T., Xie, S.P., Wittenberg, A., Sun, D.Z., 2013. Interdecadal Amplitude Modulation of El Nino-
616 Southern Oscillation and Its Impact on Tropical Pacific Decadal Variability. Journal of Climate
617 26, 7280-7297.
618 Penland, C., Sardeshmukh, P.D., 1995. The optimal growth of tropical sea surface temperature anomalies.
619 Journal of Climate 8, 1999-2024.
620 Reichler, T., Kim, J., 2008. Uncertainties in the climate mean state of global observations, reanalyses, and
621 the GFDL climate model. Journal of Geophysical Research-Atmospheres 113.

622 Roberts, W., 2007. An Investigation into the Causes for the Reduction in the Variability of the El Niño-
623 Southern Oscillation in the Early Holocene in a Global Climate Model. University of Washington,
624 Seattle, WA, p. pp 145.
625 Roberts, W.H.G., Battisti, D.S., 2011. A new tool for evaluating the physics of coupled atmosphere-ocean
626 variability in nature and in general circulation models. Climate Dynamics 36, 907-923.
627 Roberts, W.H.G., Battisti, D.S., Tudhope, A.W., 2014. ENSO in the Mid-Holocene according to CSM and
628 HadCM3. Journal of Climate 27, 1223-1242.
629 Russon, T., Tudhope, A.W., Hegerl, G.C., Schurer, A., Collins, M., 2014. Assessing the Significance of
630 Changes in ENSO Amplitude Using Variance Metrics. Journal of Climate 27, 4911-4922.
631 Takahashi, K., Dewitte, B., 2016. Strong and moderate nonlinear El Nino regimes. Clim. Dyn. 46, 1627-
632 1645.
633 Taschetto, A.S., Sen Gupta, A., Jourdain, N.C., Santoso, A., Ummenhofer, C.C., England, M.H., 2014.
634 Cold Tongue and Warm Pool ENSO Events in CMIP5: Mean State and Future Projections. J.
635 Clim. 27, 2861-2885.
636 Thompson, C.J., 1998a. Initial conditions for optimal growth in a coupled ocean-atmosphere model of
637 ENSO. Journal of the Atmospheric Sciences 55, 537-557.
638 Thompson, C.J., 1998b. A linear, stochastic, dynamical model of El Niño /Southern Oscillation. University
639 of Washington.
640 Thompson, C.J., Battisti, D.S., 2000. A linear stochastic dynamical model of ENSO. Part I: Model
641 development. Journal of Climate 13, 2818-2832.
642 Thompson, C.J., Battisti, D.S., 2001. A linear stochastic dynamical model of ENSO. Part II: Analysis.
643 Journal of Climate 14, 445-466.
644 Tudhope, A.W., Chilcott, C.P., McCulloch, M.T., Cook, E.R., Chappell, J., Ellam, R.M., Lea, D.W.,
645 Lough, J.M., Shimmield, G.B., 2001. Variability in the El Nino - Southern oscillation through a
646 glacial-interglacial cycle. Science 291, 1511-1517.
647 van Oldenborgh, G.J., Philip, S.Y., Collins, M., 2005. El Nino in a changing climate: a multi-model study.
648 Ocean Science 1, 81-95.

649 Vecchi, G.A., Wittenberg, A.T., Rosati, A., 2006. Reassessing the role of stochastic forcing in the 1997-
650 1998 El Nino. Geophys. Res. Lett. 33.
651 Vimont, D.J., 2005. The contribution of the interannual ENSO cycle to the spatial pattern of decadal
652 ENSO-like variability. J. Clim. 18, 2080-2092.
653 Watanabe, M., Kug, J.S., Jin, F.F., Collins, M., Ohba, M., Wittenberg, A.T., 2012. Uncertainty in the
654 ENSO amplitude change from the past to the future. Geophysical Research Letters 39.
655 Wittenberg, A., 2002. ENSO response to altered climates. Princeton University, p. 475.
656 Wittenberg, A., 2015. Low-frequency variations of ENSO. U.S. CLIVAR Variations 13, 26-31.
657 Wittenberg, A.T., 2009. Are historical records sufficient to constrain ENSO simulations? Geophysical
658 Research Letters 36.
659 Wittenberg, A.T., Rosati, A., Delworth, T.L., Vecchi, G.A., Zeng, F.R., 2014. ENSO Modulation: Is It
660 Decadally Predictable? Journal of Climate 27, 2667-2681.
661 Wittenberg, A.T., Rosati, A., Lau, N.C., Ploshay, J.J., 2006. GFDL's CM2 global coupled climate models.
662 Part III: Tropical pacific climate and ENSO. Journal of Climate 19, 698-722.
663 Xie, S.P., Deser, C., Vecchi, G.A., Ma, J., Teng, H.Y., Wittenberg, A.T., 2010. Global Warming Pattern
664 Formation: Sea Surface Temperature and Rainfall. J. Clim. 23, 966-986.
665 Zebiak, S.E., Cane, M.A., 1987. A model El Nino-Southern Oscillation. Monthly Weather Review 115,
666 2262-2278.
667
668
669

Table 1: ENSO characteristics in LOAM simulations.

	LOAM							CM2.1 or obs
Run name	Mean state	Variance tuned to	Noise forcing ampl. (°C) [a]	C_D [b]	Mode period (yr) [c]	Mode growth rate (yr^{-1}) [d]	Variance in LOAM [e]	Variance in CM2.1 or obs [e]
$LOAM_{EPOCH\ L} + F_M$	Epoch L	-	0.104	1.82E-3	3.2	0.49	2.2	0.7
$LOAM_{EPOCH\ M} + F_M$	Epoch M	Epoch M	0.104	1.82E-3	3.0	0.49	1.8	1.8
$LOAM_{EPOCH\ H} + F_M$	Epoch H	-	0.104	1.82E-3	3.0	0.43	1.3	3.0
$LOAM_{CM2.1} + F_M$	Epoch L,M,H avg	-	0.104	1.82E-3	3.0	0.48	1.8	1.7[f]
$LOAM_{CM2.1} + F_{CM2.1}$	Epoch L,M,H avg	4,000-yr CM2.1	0.102	1.82E-3	3.1	0.48	1.7	1.7[f]
$LOAM_{CM2.1} + F_{OBS}$	Epoch L,M,H avg	-	0.054	1.82E-3	3.1	0.48	0.5	1.7[f]
$LOAM_{OBS} + F_{OBS}$	obs	obs	0.054	1.85E-3	2.8	0.44	0.8	0.8

[a] The amplitude of the noise forcing in $LOAM_{EPOCH\ M}$ was prescribed so that the variance of Nino 3 SSTAs in LOAM matched that in CM2.1 Epoch M. This same noise forcing was used in all other LOAM simulations, aside from $LOAM_{OBS} + F_{OBS}$ and $LOAM_{CM2.1} + F_{OBS}$, in which the noise amplitude was prescribed based on the Niño 3 variance from the last 40 years of observations.

[b] Atmospheric drag coefficient (see Supplementary Material).

[c] Period of the ENSO mode.

[d] Mode growth rate, expressed as the fractional change in the amplitude of the ENSO mode over the course of a year. Growth rates less than 1 indicate damped modes.

[e] Variance of 3-month running mean Nino 3 SSTAs.

[f] Variance of Nino 3 SSTAs across 4,000 years of CM2.1

682 **Figure Captions**

683

684 **Fig. 1** Time series of 3-month running mean Niño 3 SSTAs in A) observations (ERSST.v3b, 1971-2010)
685 and CM2.1 epochs B) Epoch L, C) Epoch M, and D) Epoch H. The variance of each time series is
686 indicated in the top left corner of each panel.

687

688 **Fig. 2** Normalized EOF 1-3 of tropical Pacific SSTAs from A-C) detrended observations (ERSST.v3b,
689 1971-2010) and CM2.1 epochs D-F) Epoch L, G-I) Epoch M, and J-L) Epoch H. The fraction of total
690 SSTA variance captured by each pattern is indicated in the top left corner of each panel. ** EOF 2 and 3 in
691 Epoch M are not statistically distinguishable, based on the method of North (1982).

692

693 **Fig. 3** Variance of tropical Pacific SSTAs in A) 500 years of the CM2.1 control run and the CM2.1 epochs
694 B) Epoch L, C) Epoch M, and D) Epoch H. In subpanels (E-H), the variances are normalized with respect
695 to the maximum in each plot.

696

697 **Fig. 4** EOF 1 of tropical Pacific SSTAs from A) observations (ERSST.v3b, 1971-2010), B) 200 years of
698 LOAM run with observed mean fields, C) 200 years of the CM2.1 control-run simulation, and D) 200 years
699 of LOAM run with mean fields from CM2.1 (averaged over Epoch L, M, H). The fraction of total SSTA
700 variance captured by EOF 1 is indicated in the top left corner of each panel.

701

702 **Fig. 5** 3-month running mean Niño 3 SSTAs in A) observations (ERSST.v3b, 1880 – 2010), B) 130 years
703 of the 2,000-year LOAM with mean states from observations, C) 130 years of the 4,000-year control run of
704 CM2.1, and D) 130 years of the 4,000-year LOAM with mean states from CM2.1 (averaged over Epoch L,
705 M, H). The variance of each complete time series is indicated in the top left corner of each panel. Only the
706 last 50 years of observational data was used to calculate the variance in panel (A), as only the period from
707 1961-2010 was used to tune the $LOAM_{OBS}$ run.

708

Fig. 6 Cumulative probability distributions of Niño 3 SSTAs in detrended observations (black; NOAA ERSST v3b, 1880 – 2011 AD), 2,000 years of the CM2.1 control run (red). Gaussian distributions with the mean and standard deviation estimated from the data are plotted as dashed lines. The $LOAM_{OBS}$ and $LOAM_{CM2.1}$ curves have been omitted for clarity, but overlay the Gaussian distributions fit to observations and CM2.1, respectively.

Fig. 7 Power spectra of 3-month running mean Niño 3 SSTAs in observations (solid black; NOAA ERSST.v3b, 1880 – 2011), the 4,000-year LOAM tuned to observations (dashed black), the 4,000-year control run of CM2.1 (solid grey) and the 4,000-year LOAM tuned to CM2.1 (dashed grey). The power spectra were computed using a forward Fast Fourier Transform; they preserve variance so that the area under the curve equals the variance of the detrended Niño 3 timeseries.

Fig. 8 Variance of 3-month running mean Niño 3 SSTAs as a function of month in A) observations (ERSST.v3b, 1880-2010), B) the 4,000 year LOAM with observed mean states, C) the 4,000 year CM2.1 control run, and D) the 4,000 year LOAM run with CM2.1 mean states.

Fig. 9 A) Mean annual tropical Pacific SST and near-surface winds in CM2.1 Epoch M and differences in mean surface winds between CM2.1 epochs: B) Epoch L – M; C) Epoch H – M.

Fig. 10 Differences in mean annual equatorial Pacific upper ocean temperature profiles (colors; averaged between 2°S:2°N) in CM2.1 epochs: A) Epoch L - M and B) Epoch H – M. Unfilled contours are the mean annual equatorial temperature in Epoch M. The contour interval is 2°C and the bold contour is the 20°C isotherm.

Fig. 11 Variance of Niño 3 SSTAs in LOAM versus CM2.1. The LOAM simulations correspond to $LOAM_{EPOCH\ L} + F_M$, $LOAM_{EPOCH\ M} + F_M$, $LOAM_{EPOCH\ H} + F_M$ and $LOAM_{CM2.1} + F_M$ in Table 1. The diameter of the data points is proportional to the growth rate of the ENSO mode. The dotted 1:1 line is plotted for visual reference.

737

738 **Fig. 12** Probability distributions of 40-year variance of Niño 3 SSTAs (bars) plotted with $\chi 2$ distributions
739 (lines) for the 4,000-year CM2.1 run (black), the 4,000-year $LOAM_{CM2.1}+F_{CM2.1}$ run (blue), the 4,000-year
740 $LOAM_{OBS}+F_{OBS}$ run (red), and the 4,000-year $LOAM_{CM2.1}+ F_{OBS}$ run (green). The $\chi 2$ distributions were
741 calculated using Eqns. (1)-(2). The grey shaded bar represents the range of observed variance in 40-yr
742 intervals across the 20th century and the vertical line represents the observed variance during the period
743 1961-2010 (from NOAA ERSST v3b 1961-2010). B) PDFs from subpanel (A) converted into relative
744 differences in variance, with respect to the long-term variance in each simulation.

745

746 **Fig. 13** Monthly zonal wind stress anomalies in the western Pacific (left column) and central Pacific (right
747 column) versus Niño 3 SSTAs in 500 years of the CM2.1 control simulation (top row) or observations
748 (bottom row; 1958-2001; SODA zonal windstress and ERSST v3b SST data). The CM2.1 data are divided
749 into two subsets- the "high variance epochs" subset contains data from periods in which the 40-year
750 running mean variance of Niño 3 SSTAs $\geq 2.0°C^2$, while the "low variance epochs" subset contains data
751 from periods in which the 40-year running mean variance of Niño 3 SSTAs $\leq 1.0°C^2$. For the WP data (left
752 column) zonal wind anomalies were averaged over the Niño 4 region (160°E:150°W, 5°S:5°N) for
753 observations and over 150°E:160°W, 5°S:5°N for CM2.1 (representing the region of peak zonal wind
754 anomalies in each data set). For the CP data (right column), the zonal wind anomalies were averaged over
755 the Nino 3.4 region (170°W:120°E, 5°S:5°N) for both CM2.1 and observations.

756

757 **Fig. 14** Skewness of tropical Pacific zonal wind stress anomalies in A) 500 years of the CM2.1 control
758 simulation; B) observations (SODA v2.0.2-4, 1958-2007); C) low variance epochs in CM2.1 and D) high
759 variance epochs in CM2.1. The CM2.1 data are divided into two subsets- the "low variance epochs" subset
760 (C) contains data from periods in which the 40-year running mean variance of Niño 3 SSTAs $\leq 1.0°C^2$
761 while the "high variance epochs" subset (D) contains data from periods in which the 40-year running mean
762 variance of Niño 3 SSTAs $\geq 2.0°C^2$.

763

764 **Fig. 15** As in Fig. 14, but for SSTAs. Observational data is from ERSST.v3b, for the period 1951-2010.

Figure

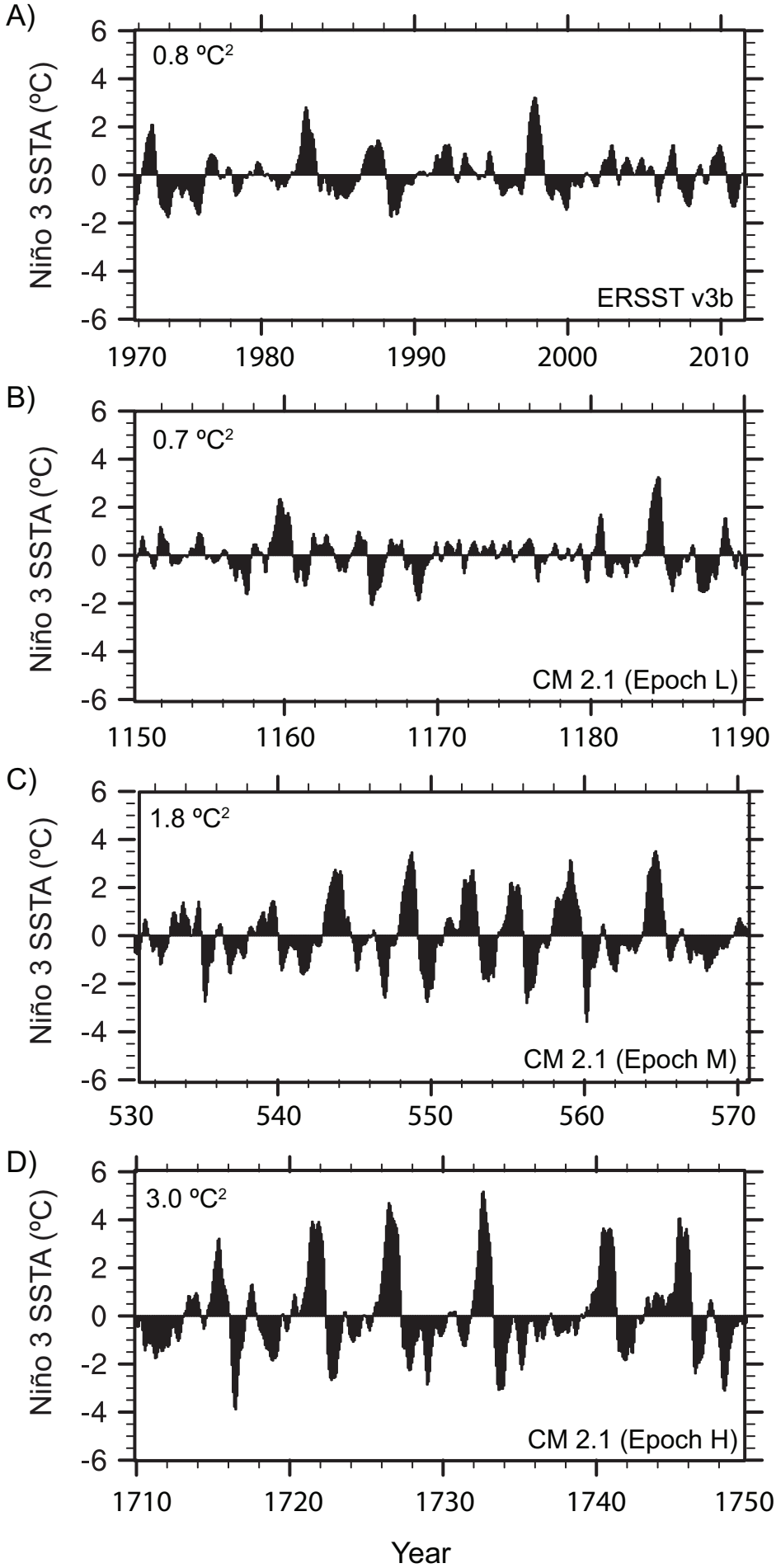

Fig. 1 Time series of 3-month running mean Niño 3 SSTAs in A) observations (ERSST.v3b, 1971-2010) and CM2.1 epochs B) Epoch L, C) Epoch M, and D) Epoch H. The variance of each time series is indicated in the top left corner of each panel.

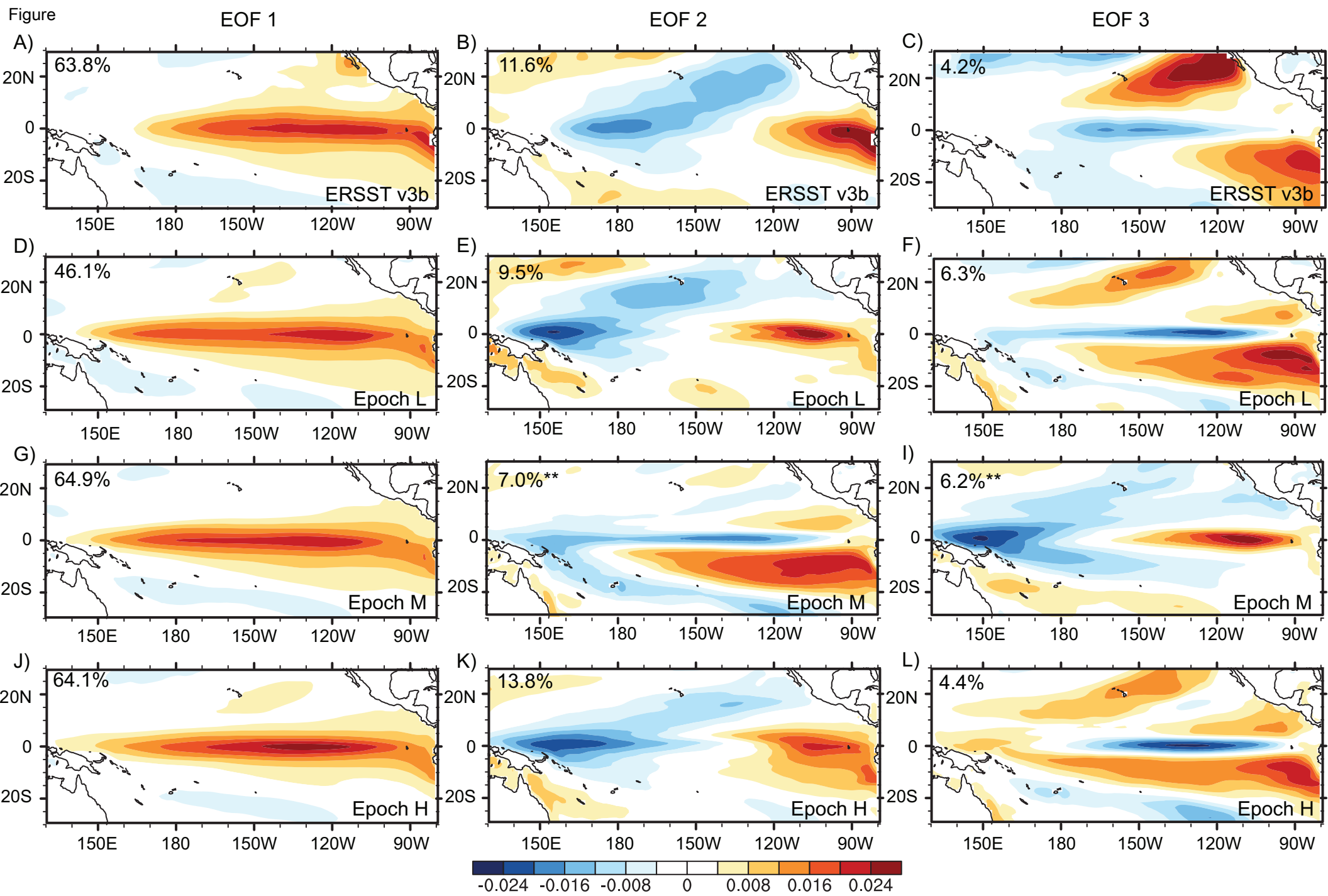

Fig. 2 Normalized EOF 1-3 of tropical Pacific SSTAs from A-C) detrended observations (ERSST.v3b, 1971-2010) and CM2.1 epochs D-F) Epoch L, G-I) Epoch M, and J-L) Epoch H. The fraction of total SSTA variance captured by each pattern is indicated in the top left corner of each panel. ** EOF 2 and 3 in Epoch M are not statistically distinguishable, based on the method of North (1982).

Figure

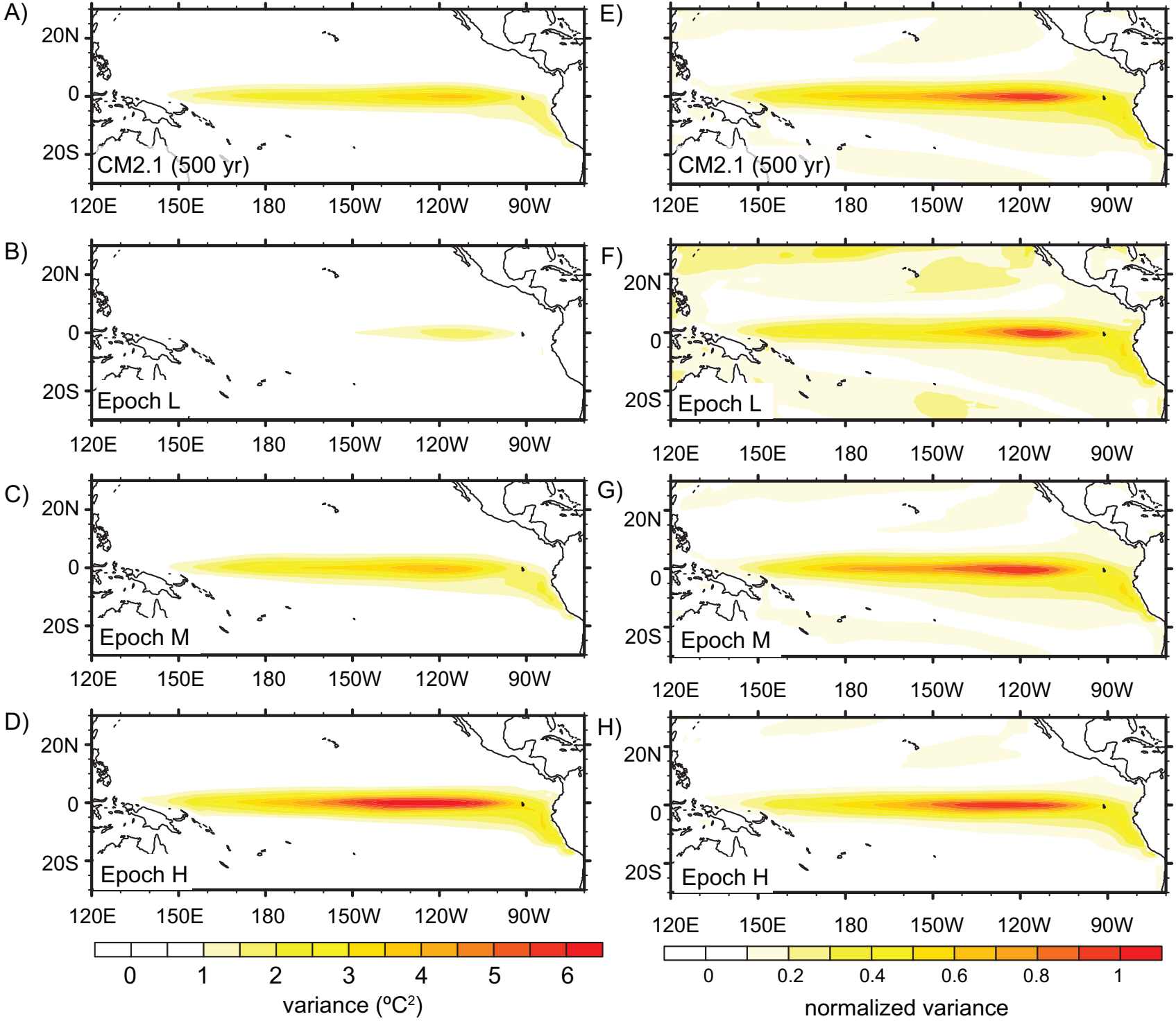

Fig. 3 Variance of tropical Pacific SSTAs in A) 500 years of the CM2.1 control run and the CM2.1 epochs B) Epoch L, C) Epoch M, and D) Epoch H. In subpanels (E-H), the variances are normalized with respect to the maximum in each plot.

Figure

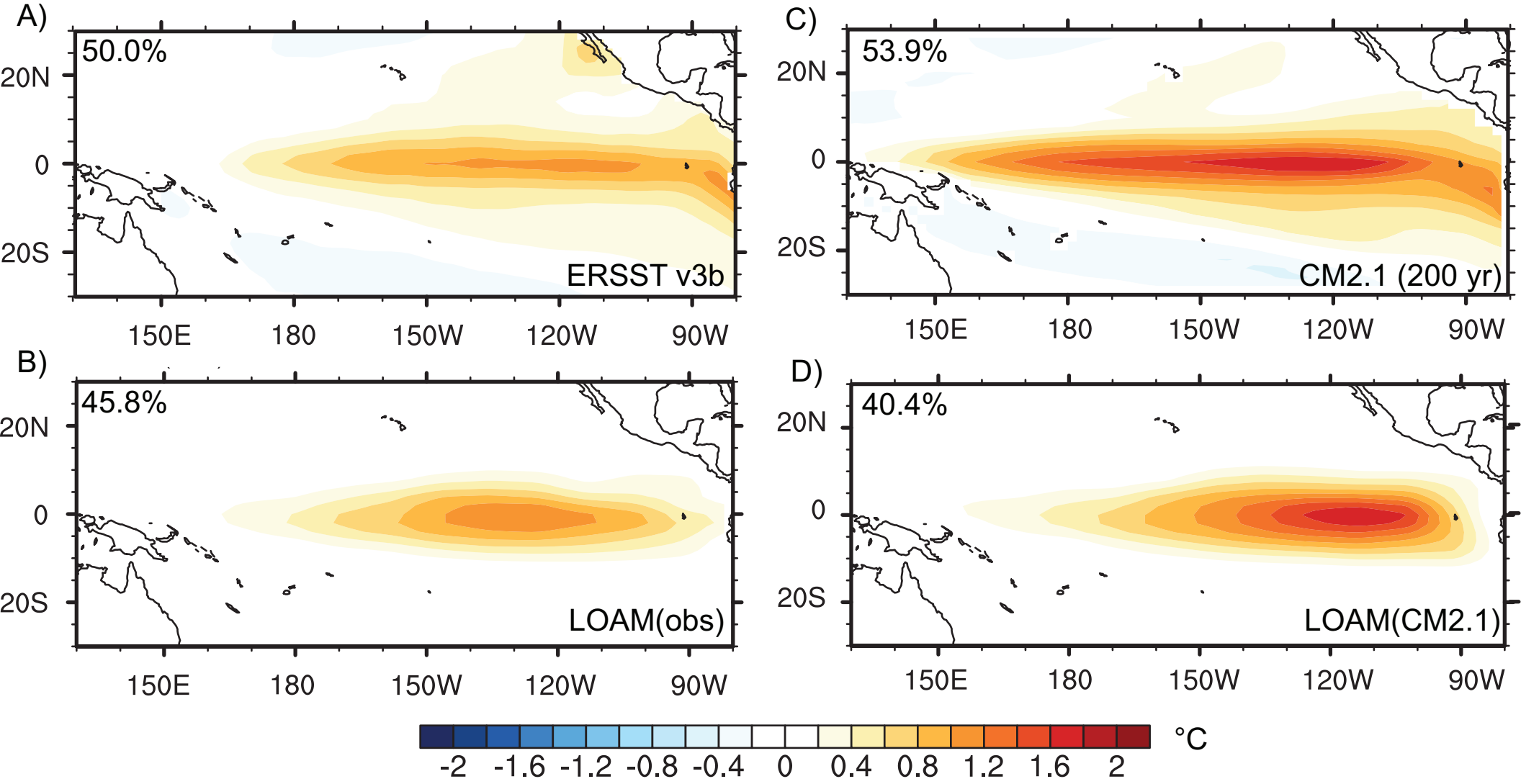

Fig. 4 EOF 1 of tropical Pacific SSTAs from A) observations (ERSST.v3b, 1971-2010), B) 200 years of LOAM run with observed mean fields, C) 200 years of the CM2.1 control-run simulation, and D) 200 years of LOAM run with mean fields from CM2.1 (averaged over Epoch L, M, H). The fraction of total SSTA variance captured by EOF 1 is indicated in the top left corner of each panel.

Figure

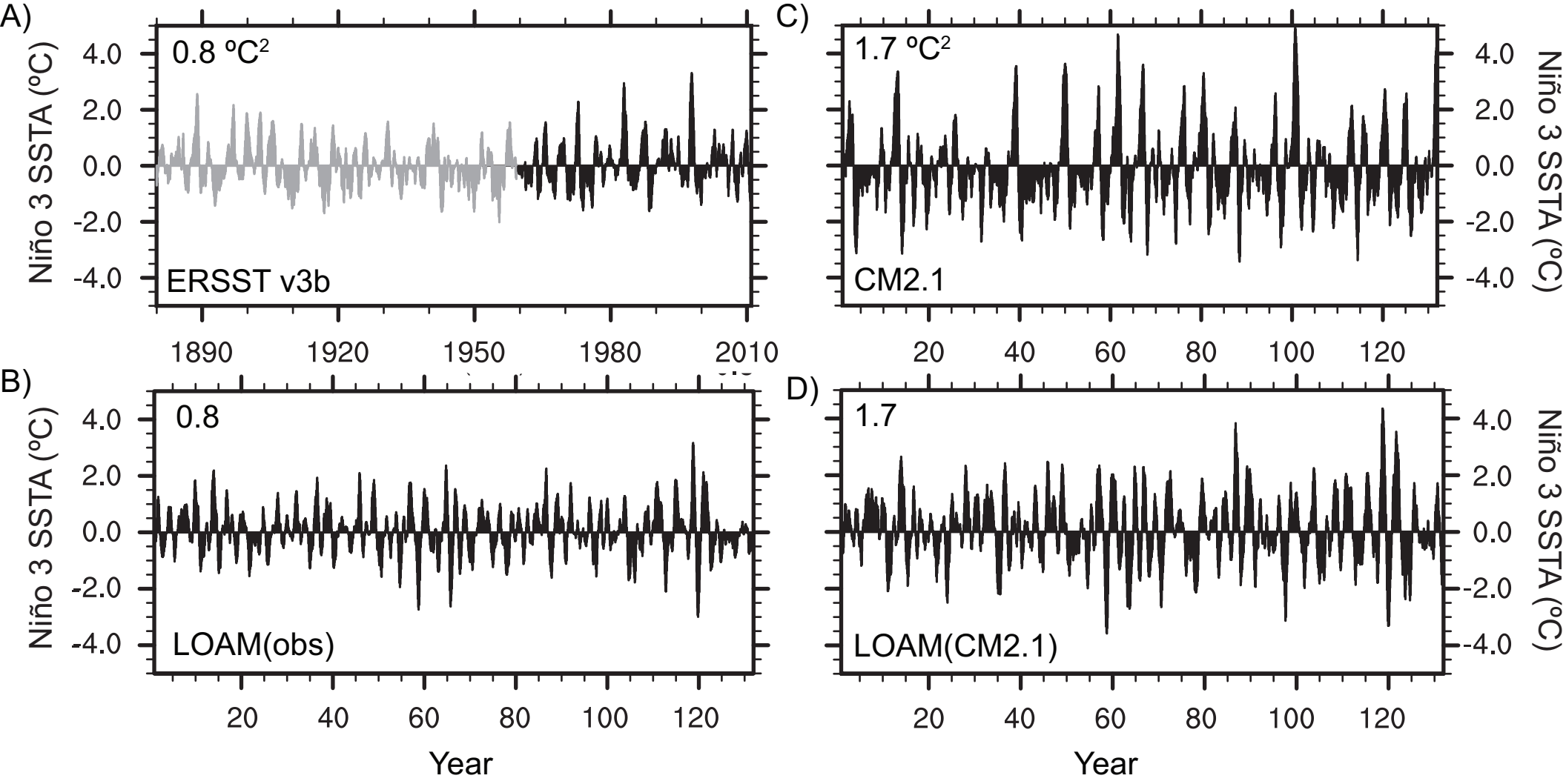

Fig. 5 3-month running mean Niño 3 SSTAs in A) observations (ERSST.v3b, 1880 – 2010), B) 130 years of the 4,000-year LOAM with mean states from observations, C) 130 years of the 4,000-year control run of CM2.1, and D) 130 years of the 4,000-year LOAM with mean states from CM2.1 (averaged over L, M, H). The variance of each complete time series is indicated in the top left corner of each panel. Only the last 50 years of observational data was used to calculate the variance in panel (A), as only the period from 1961-2010 was used to tune the $LOAM_{OBS}$ run.

Figure

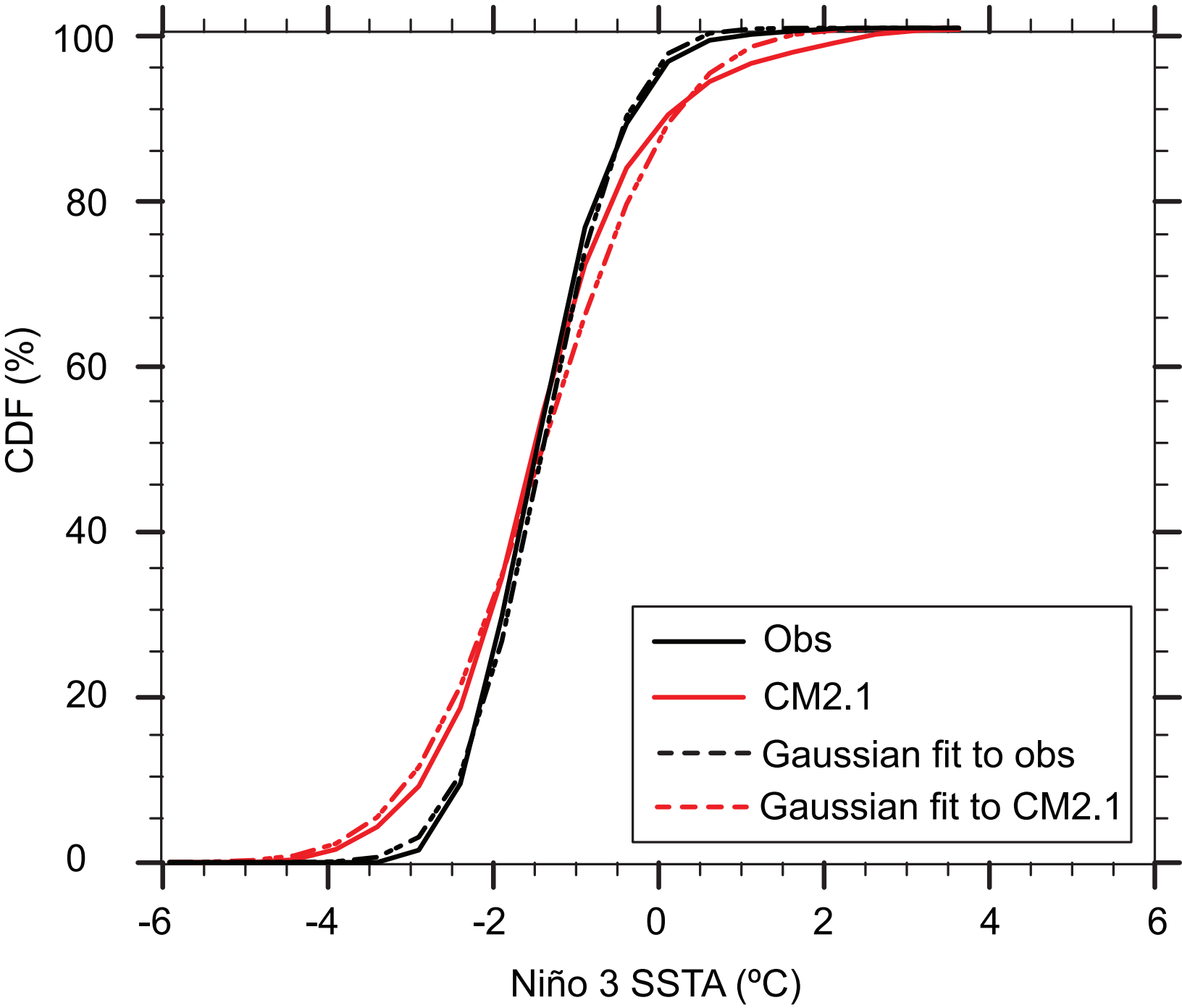

Fig. 6 Cumulative probability distributions of Niño 3 SSTAs in detrended observations (black; NOAA ERSST v3b, 1880 – 2011 AD), 2,000 years of the CM2.1 control run (red). Gaussian distributions with the mean and standard deviation estimated from the data are plotted as dashed lines. The $LOAM_{obs}$ and $LOAM_{CM2.1}$ curves have been omitted for clarity, but perfectly overlay the Guassian distributions fit to observations and CM2.1, respectively.

Figure

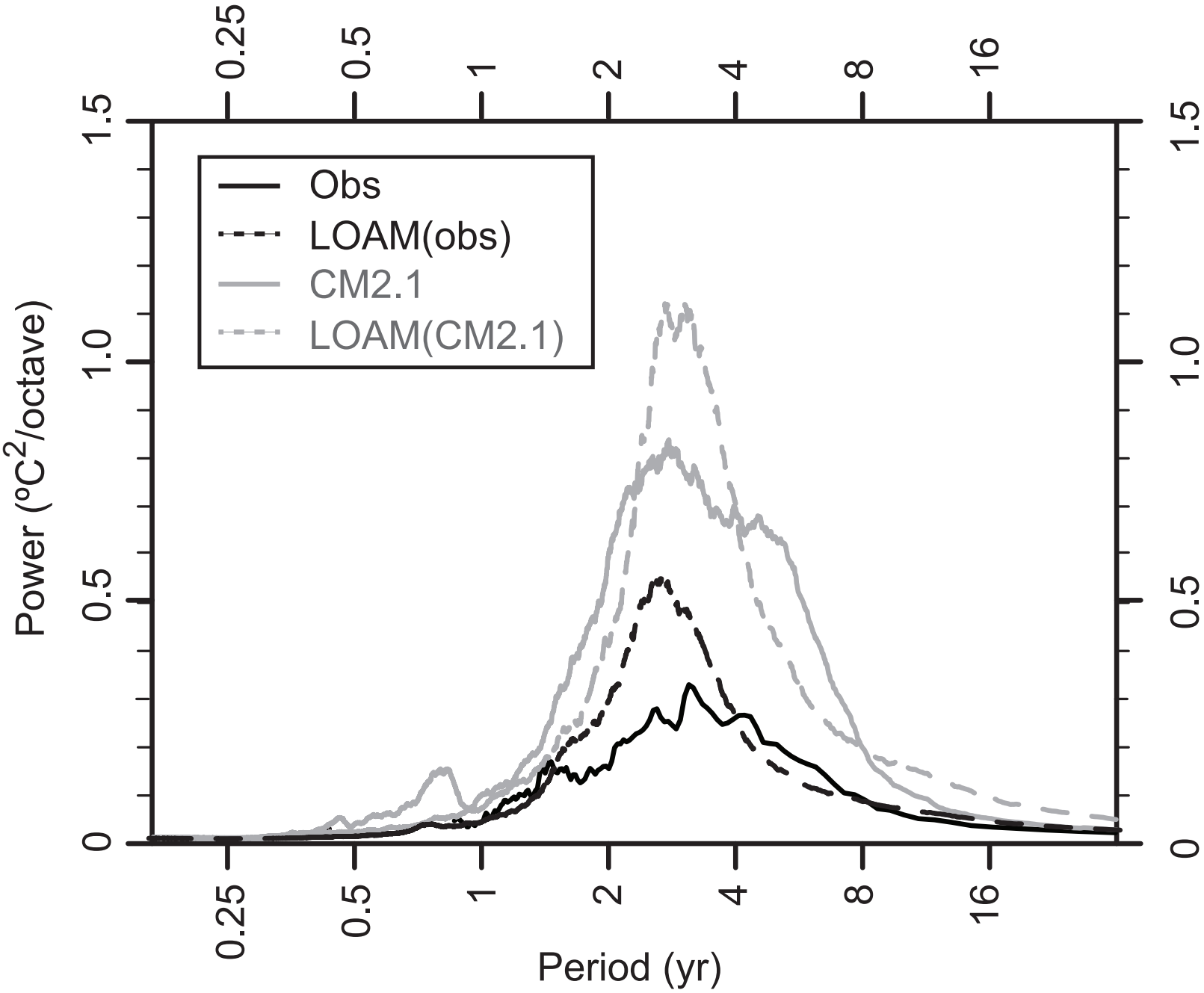

Fig. 7 Power spectra of 3-month running mean Niño 3 SSTAs in observations (solid black; NOAA ERSST.v3b, 1880–2011), the 4,000-year LOAM tuned to observations (dashed black), the 4,000-year control run of CM2.1 (solid grey) and the 4,000-year LOAM tuned to CM2.1 (dashed grey). The power spectra were computed using a forward Fast Fourier Transform; they preserve variance so that the area under the curve equals the variance of the detrended Niño 3 timeseries.

Figure

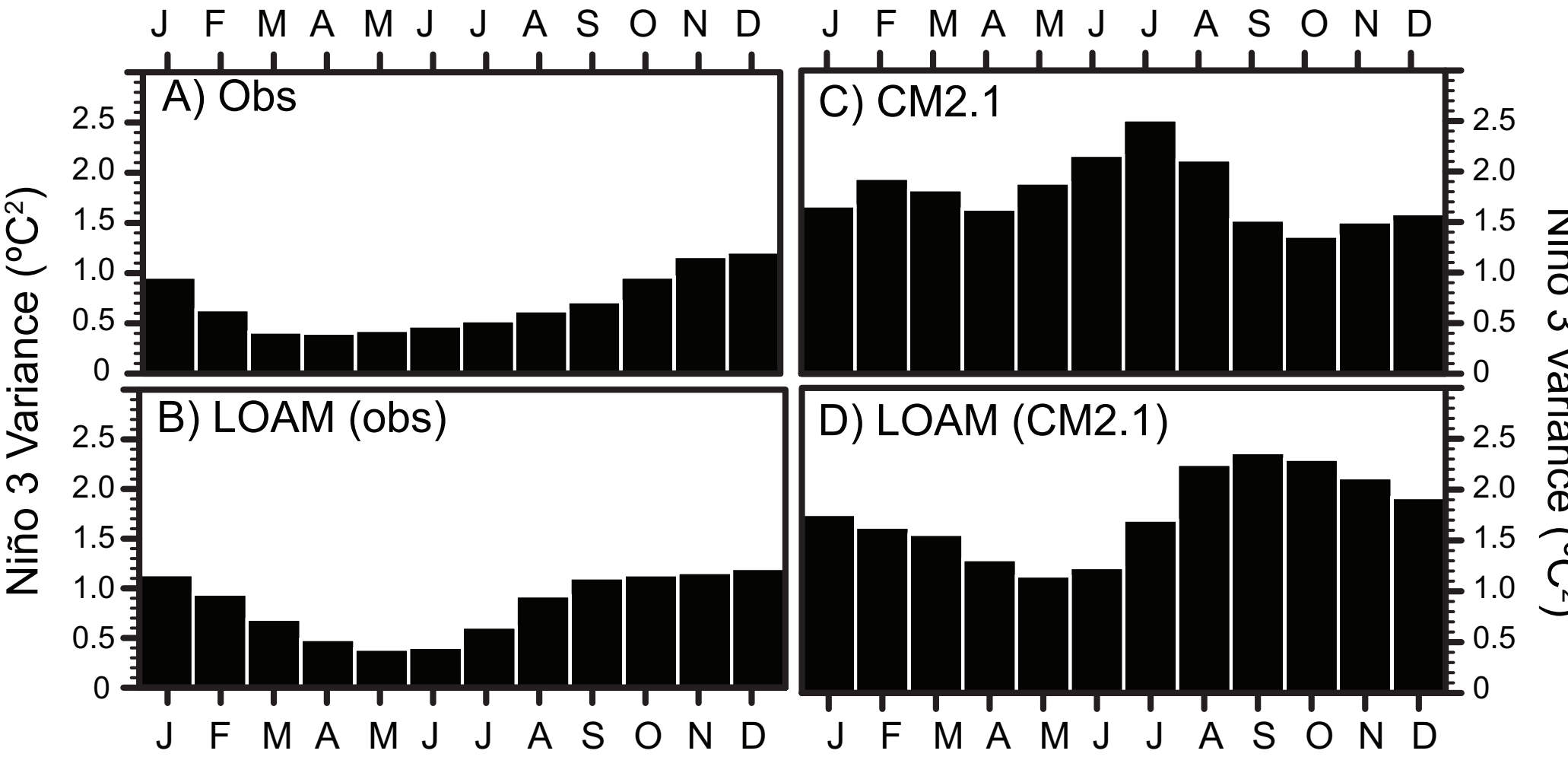

Fig. 8 Variance of 3-month running mean Niño 3 SSTAs as a function of month in A) observations (ERSST.v3b, 1880-2010), B) the 4,000 year LOAM with observed mean states, C) the 4,000 year CM2.1 control run, and D) the 4,000 year LOAM run with CM2.1 mean states.

Figure

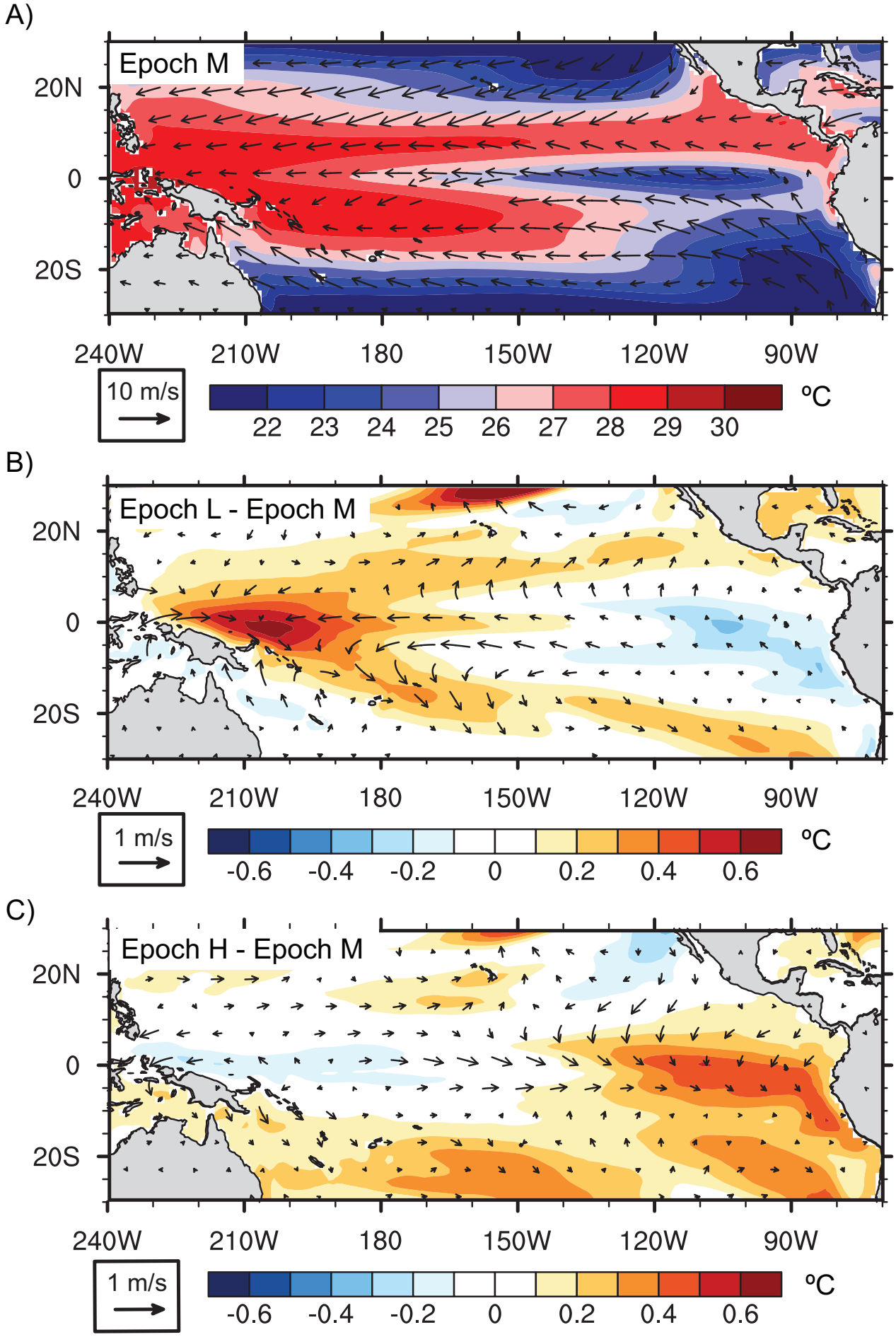

Fig. 9 A) Mean annual tropical Pacific SST and near-surface winds in CM2.1 Epoch M and differences in mean surface winds between CM2.1 epochs: B) Epoch L – M; C) Epoch H – M.

Figure

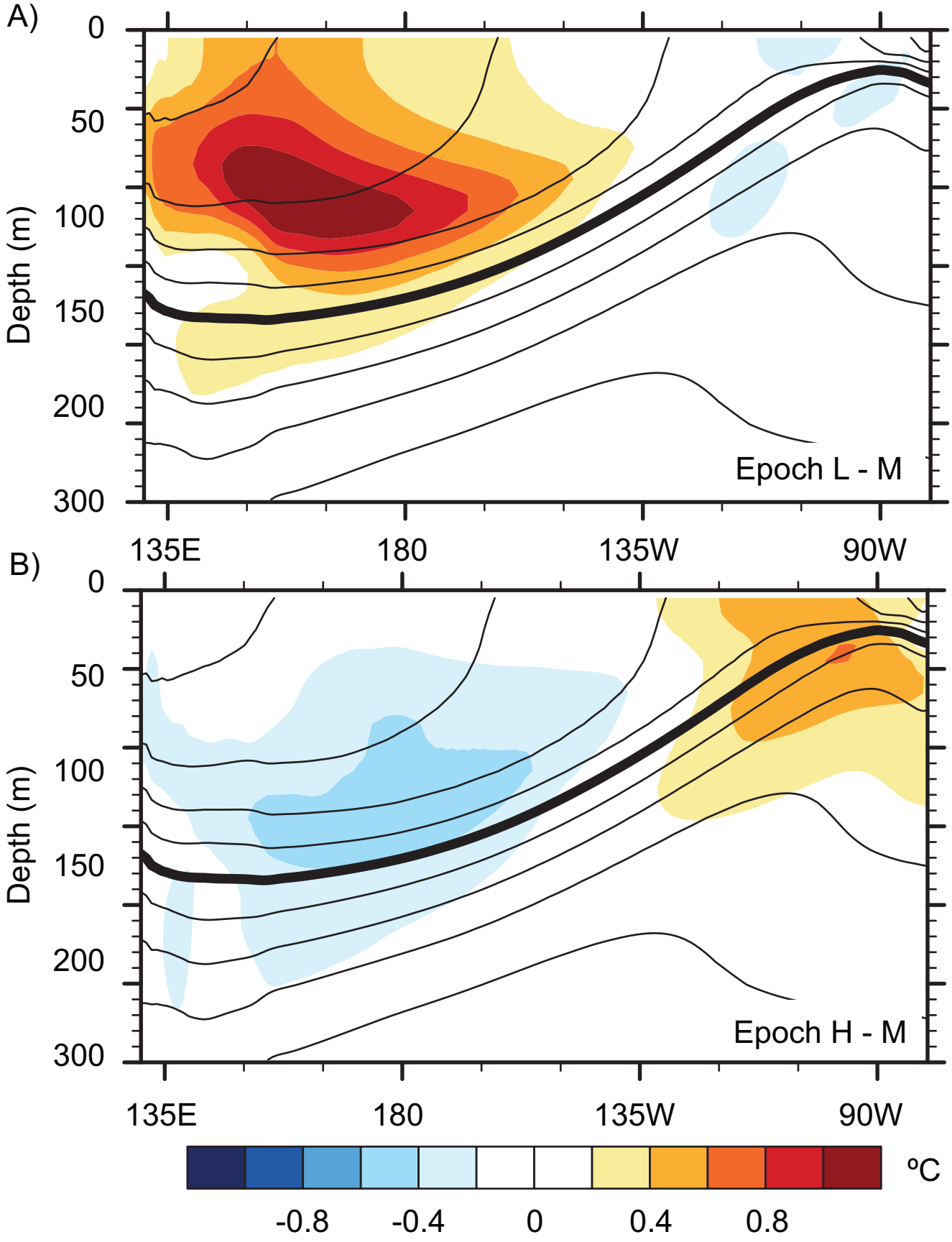

Fig. 10 Differences in mean annual equatorial Pacific upper ocean temperature profiles (colors; averaged between 2°S:2°N) in CM2.1 epochs: A) Epoch L - M and B) Epoch H – M. Unfilled contours are the mean annual equatorial temperature in Epoch M. The contour interval is 2°C and the bold contour is the 20°C isotherm.

Figure

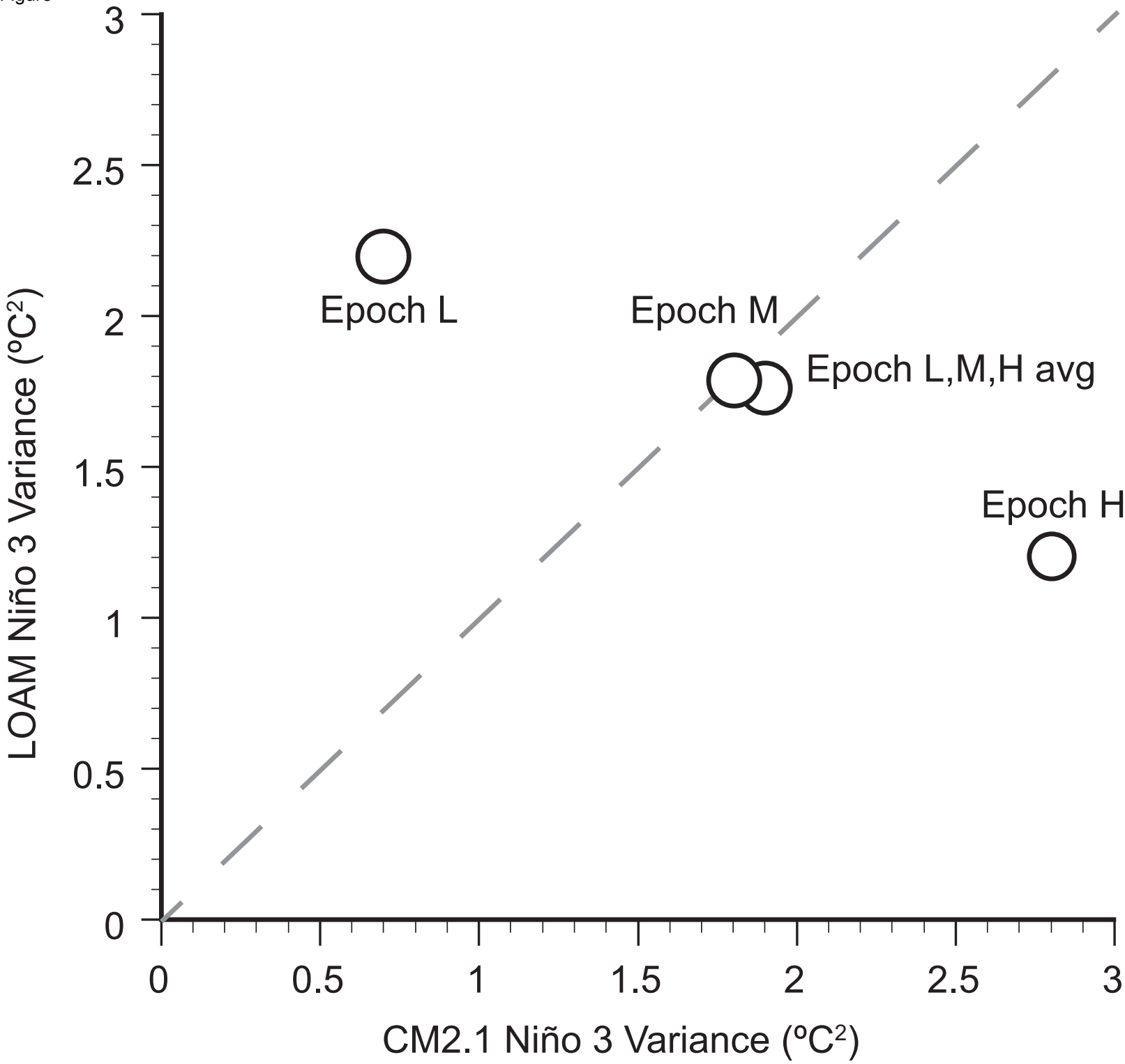

Fig. 11 Variance of Niño 3 SSTAs in LOAM versus CM2.1. The LOAM simulations correspond to $LOAM_{Epoch\ L} + F_{M'}$ $LOAM_{Epoch\ M} + F_{M'}$ $LOAM_{Epoch\ H} + F_{M}$ and $LOAM_{CM2.1} + F_{M}$ in Table 1. The diameter of the data points is proportional to the growth rate of the ENSO mode. The dotted 1:1 line is plotted for visual reference.

Figure

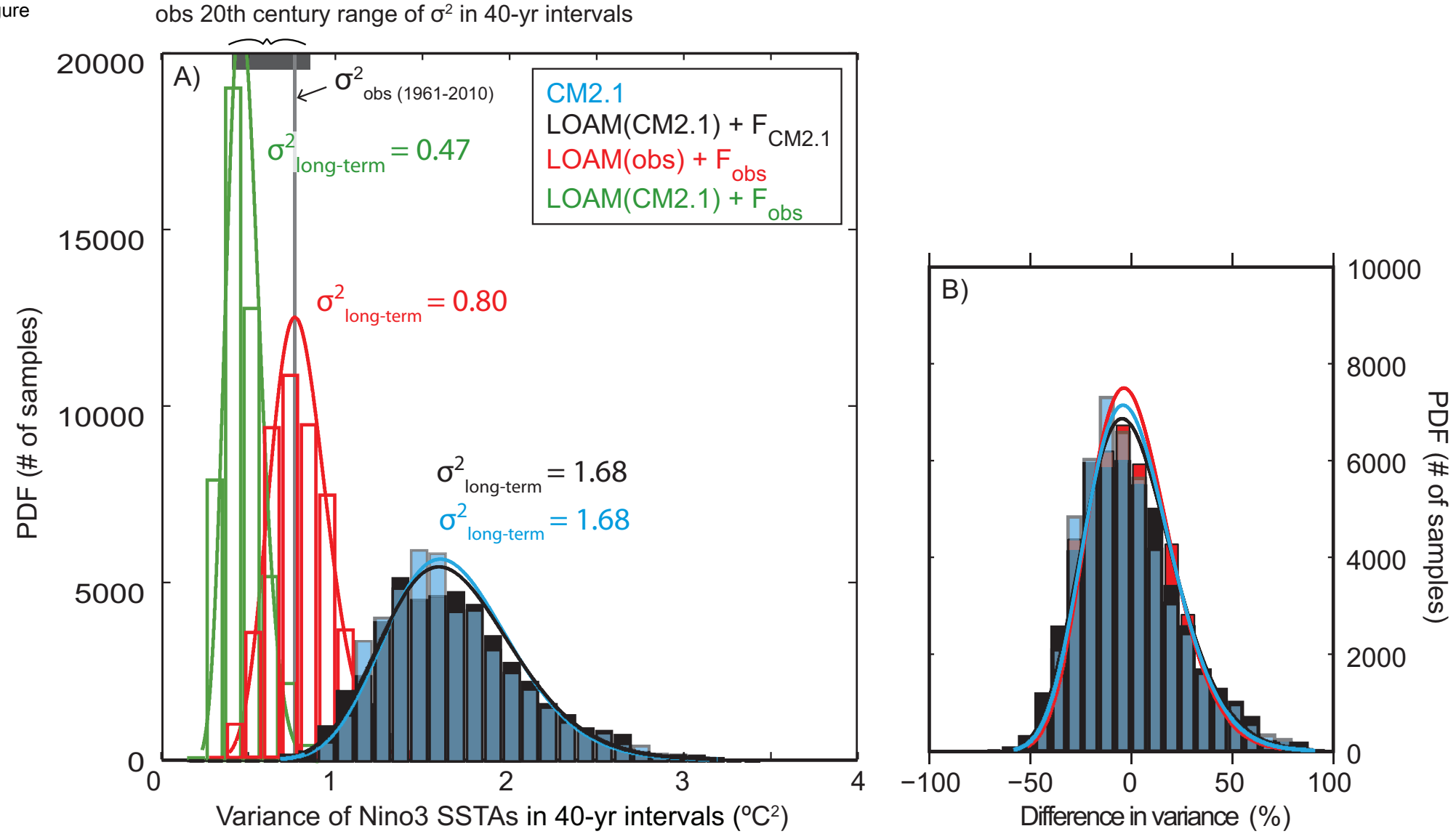

Fig. 12 A) Probability distributions of 40-year variance of Niño 3 SSTAs (bars) plotted with χ2 distributions (lines) for the 4,000-year CM2.1 run (blue), the 4,000-year LOAM $_{CM2.1}$+F$_{CM2.1}$ run (black), the 4,000-year LOAM$_{OBS}$+F$_{OBS}$ run (red), and the 4,000-year LOAM$_{CM2.1}$+F$_{OBS}$ run (green). The χ2 distributions were calculated using Eqns. (1)-(2). The grey shaded bar represents the range of observed variance in 40-yr intervals across the 20th century and the vertical line represents the observed variance during the period 1961-2010 (from NOAA ERSST v3b 1961-2010). B) PDFs from subpanel (A) converted into relative differences in variance, with respect to the long-term variance in each simulation.

Figure

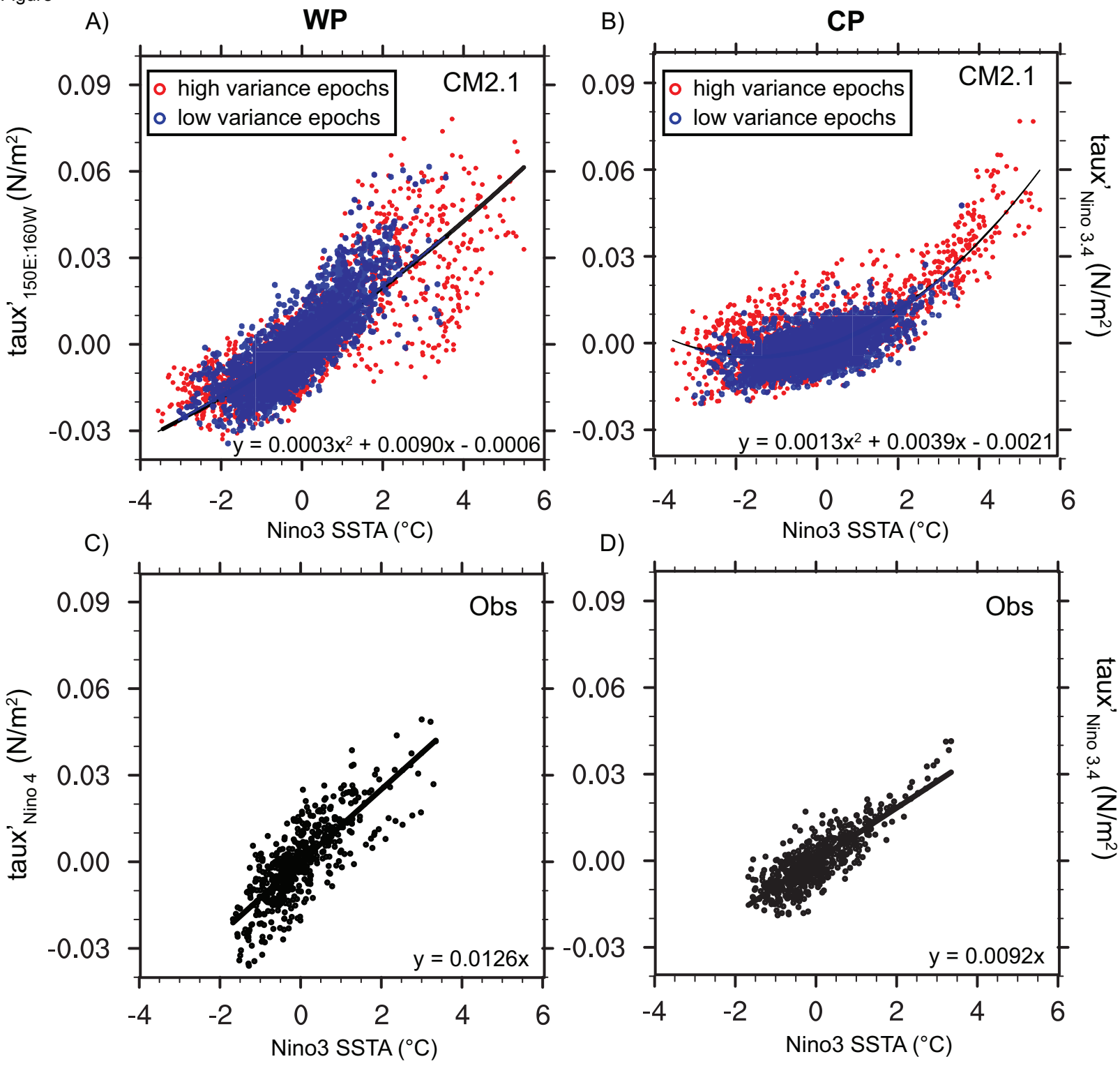

Fig. 13 Monthly zonal wind stress anomalies in the western Pacific (left column) and central Pacific (right column) versus Niño 3 SSTAs in 500 years of the CM2.1 control simulation (top row) or observations (bottom row; 1958-2001; SODA zonal windstress and ERSST v3b SST data). The CM2.1 data are divided into two subsets- the "high variance epochs" subset contains data from periods in which the 40-year running mean variance of Niño 3 SSTAs ≥ 2.0°C^2, while the "low variance epochs" subset contains data from periods in which the 40-year running mean variance of Niño 3 SSTAs ≤ 1.0°C^2. For the WP data (left column) zonal wind anomalies were averaged over the Niño 4 region (160°E:150°W, 5°S:5°N) for observations and over 150°E:160°W, 5°S:5°N for CM2.1 (representing the region of peak zonal wind anomalies in each data set). For the CP data (right column), the zonal wind anomalies were averaged over the Nino 3.4 region (170°W:120°E, 5°S:5°N) for both CM2.1 and observations.

Figure

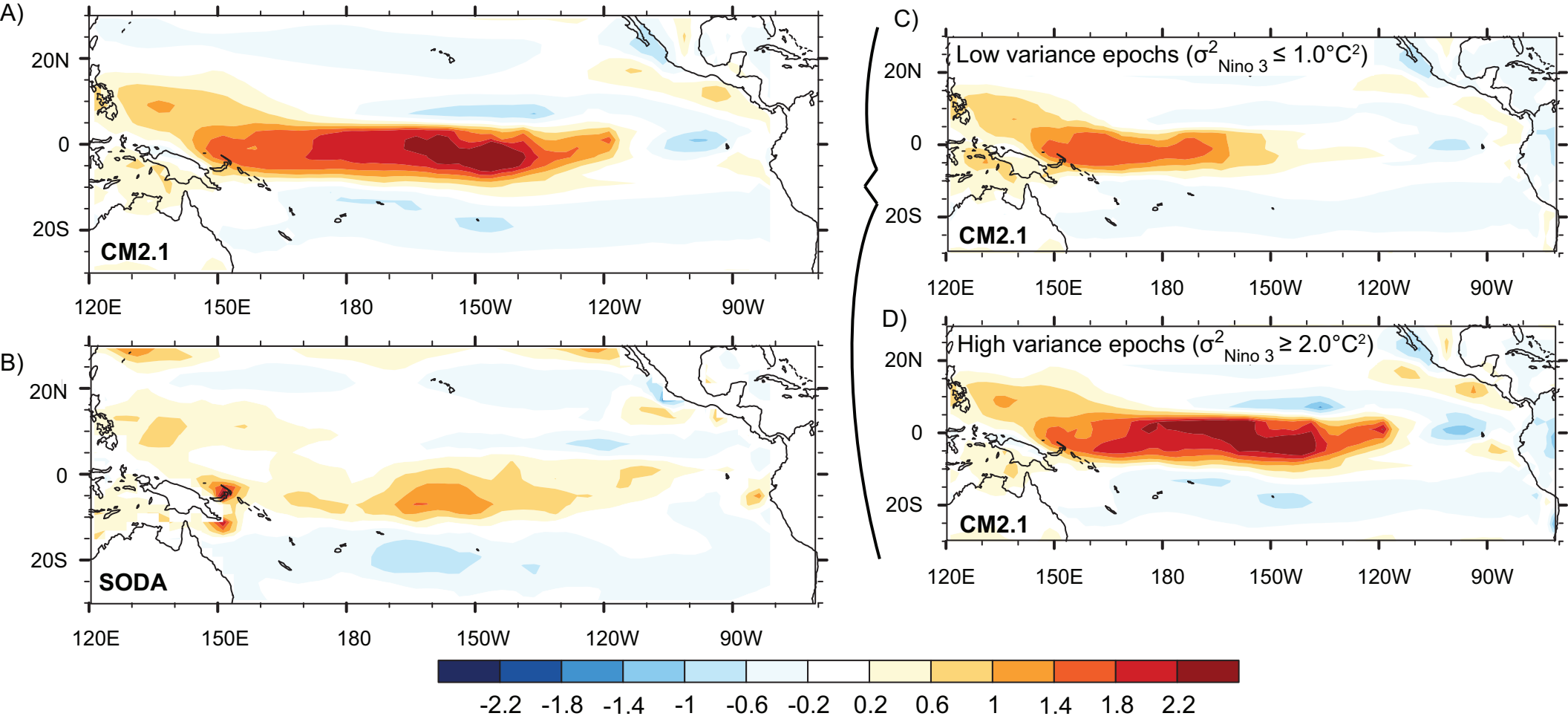

Fig. 14 Skewness of tropical Pacific zonal wind stress anomalies in A) 500 years of the CM2.1 control simulation; B) observations (SODA v2.0.2-4, 1958-2007); C) low variance epochs in CM2.1 and D) high variance epochs in CM2.1. The CM2.1 data are divided into two subsets- the “low variance epochs” subset (C) contains data from periods in which the 40-year running mean variance of Niño 3 SSTAs ≤ 1.0°C2 while the “high variance epochs” subset (D) contains data from periods in which the 40-year running mean variance of Niño 3 SSTAs ≥ 2.0°C2.

Figure

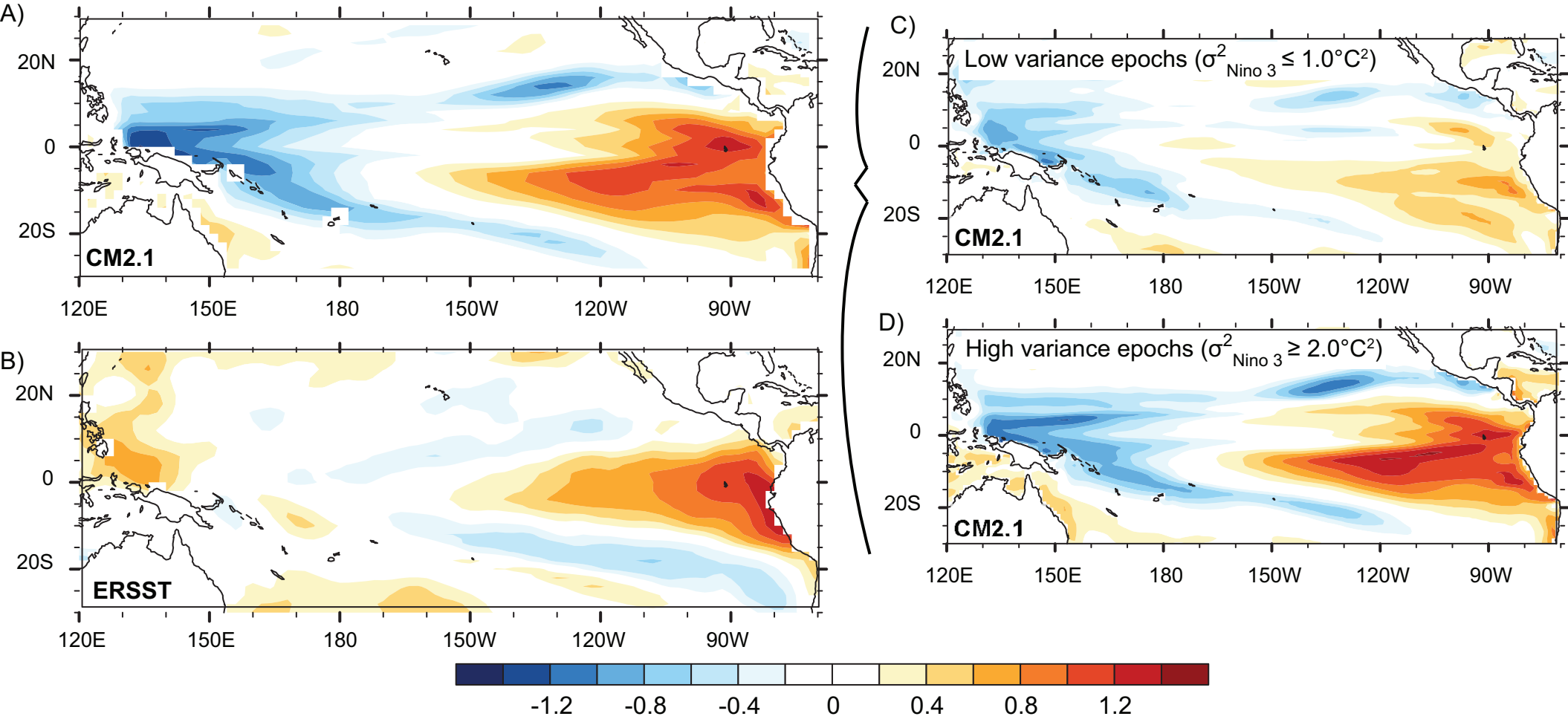

Fig. 15 As in Fig. 16, but for SSTAs. Observational data is from ERSST.v3b, for the period 1951-2010.